

Journal Pre-proofs

Significance of external wind conditions on the convective heat transfer coefficients (CHTC) and energy performance in multi-zone high-rise buildings

Kemin Ding, John Kaiser Calautit, Carlos Jimenez-Bescos

PII: S0378-7788(24)00686-8
DOI: <https://doi.org/10.1016/j.enbuild.2024.114570>
Reference: ENB 114570

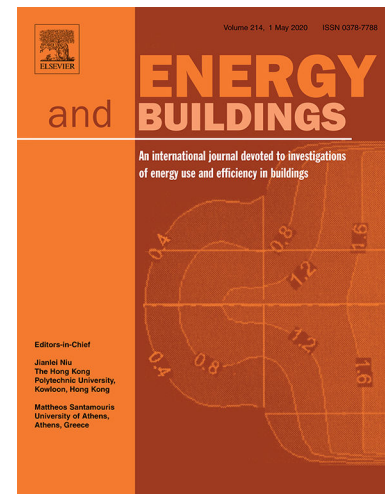
To appear in: *Energy & Buildings*

Received Date: 22 March 2024
Revised Date: 27 June 2024
Accepted Date: 15 July 2024

Please cite this article as: K. Ding, J. Kaiser Calautit, C. Jimenez-Bescos, Significance of external wind conditions on the convective heat transfer coefficients (CHTC) and energy performance in multi-zone high-rise buildings, *Energy & Buildings* (2024), doi: <https://doi.org/10.1016/j.enbuild.2024.114570>

This is a PDF file of an article that has undergone enhancements after acceptance, such as the addition of a cover page and metadata, and formatting for readability, but it is not yet the definitive version of record. This version will undergo additional copyediting, typesetting and review before it is published in its final form, but we are providing this version to give early visibility of the article. Please note that, during the production process, errors may be discovered which could affect the content, and all legal disclaimers that apply to the journal pertain.

© 2024 Published by Elsevier B.V.



Significance of external wind conditions on the convective heat transfer coefficients (CHTC) and energy performance in multi-zone high-rise buildings

Kemin Ding^{a*}, John Kaiser Calautit^a, Carlos Jimenez-Bescos^b

^a*Department of Architecture and Built Environment, University of Nottingham, NG7 2RD, UK*

^b*School of Applied Management, University of Westminster, NW1 5LS, UK*

*corresponding author email: laykd2@nottingham.ac.uk

Abstract

The study investigates the impact of external wind conditions on the convective heat transfer coefficients (CHTC) and overall energy performance in multi-zone high-rise buildings. The research employs a coupling method between building energy simulation (BES) and computational fluid dynamics (CFD) tools to enhance the accuracy of CHTC calculations. The methodology integrates meteorological and microclimate data, emphasizing detailed wind direction captured through Building Controls Virtual Test Bed (BCVTB) and MATLAB scripts. The high-rise building model was tested across various global cities with distinct climatic conditions. The coupling method significantly improves CHTC predictions compared to conventional algorithms such as DOE-2, TARP, MoWiTT, and Adaptive Convection Algorithm. Notably, the coupling method revealed substantial underestimations in traditional models, particularly in winter scenarios, with CHTC values up to 102.26% higher. This discrepancy highlights the importance of dynamic modeling approaches that incorporate detailed wind data and façade orientations. Among various algorithms, the Simple Combined algorithm calculates 4.30% lower energy demand compared with coupling method, while others estimate higher, DOE-2 has a 5.76% overestimation, followed by MoWiTT with 6.77%, TARP with 9.37%, and the Adaptive Convection Algorithm with 12.63%. This study provides robust data and insights that could inform design optimization and energy conservation strategies, making it crucial for advancing high-rise building energy modeling. The research highlights the necessity for improved BES tools to optimize thermal performance, reduce energy consumption, and enhance comfort in high-rise buildings under diverse climatic conditions.

Keywords: building; building energy simulation; CFD; convective heat transfer coefficient; wind

Highlights

- Coupled BES-CFD model reveals CHTC inaccuracies in high-rise building simulations.
- Coupling method can predict up to 102.26% higher CHTC values than DOE-2 algorithm.
- Greater CHTC variations observed in winter, especially for windward façades.
- Coupling method impacts external wall heat balance, affecting wall temperatures.
- Coupling method shows energy demand discrepancies compared to empirical algorithms.

Nomenclature

Latin Symbols

a MoWiTT coefficients (multiplier)

A Surface area [m^2]

b	MoWiTT coefficients (exponent)
C_t	Turbulent natural convection constant
C_μ	Constant, equal to 0.09
D	Material roughness coefficient
D_ω	Cross-diffusion term
E	Material roughness coefficient
E_r	Radius of the Earth, equal to 6,356 km
E_{total}	Total energy [J]
F	Material roughness coefficient
\vec{F}_b	Body forces [N]
F_{air}	View factor of wall surface to air
F_{gnd}	View factor of wall surface to ground
F_{sky}	View factor of wall surface to sky
\tilde{G}_k	Generation of turbulence kinetic energy due to mean velocity gradients [$kg/(m \cdot s^3)$]
G_ω	Generation of ω [$kg/(m \cdot s^3)$]
h	Heat transfer coefficient [$W/(m^2 \cdot K)$]
$h_{c,ext}$	Exterior convection heat transfer coefficient [$W/(m^2 \cdot K)$]
$h_{c,glass}$	Exterior convection heat transfer coefficient for smooth surfaces [$W/(m^2 \cdot K)$]
h_f	Forced convection heat transfer coefficient [$W/(m^2 \cdot K)$]
h_j	Species enthalpy of species j [J/kg]
h_n	Natural convection heat transfer coefficient [$W/(m^2 \cdot K)$]
i	Inside surface of the building element
I	Turbulent intensity
j	Time step index
\vec{j}_j	Diffusion flux of species j [$kg/(m^2 \cdot s)$]
k	Turbulence kinetic energy [m^2/s^2]
k_{eff}	Effective conductivity [$W/(m \cdot K)$]

L	Air temperature gradient, equal to -0.0065 K/m
o	Outside surface of the building element
q''_{asol}	Absorbed direct and diffuse solar radiation heat flux [W/m^2]
q''_{conv}	Convection flux [W/m^2]
q''_{LWR}	Net longwave radiation flux [W/m^2]
q''_{ko}	Conduction heat flux [W/m^2]
p	Static pressure [Pa]
P	Perimeter of surface [m]
R_f	Surface roughness multiplier
S_h	User-defined heat sources [W]
S_k	Source term for k [$kg/(m^3 \cdot s)$]
S_m	User-defined mass sources [$kg/(m^3 \cdot s)$]
S_ω	Source term for ω [$kg/(m^3 \cdot s)$]
t	Current time step [s]
T	Temperature [$^{\circ}C$]
ΔT	Temperature difference between the surface and air [$^{\circ}C$]
T_{air}	Outside air temperature [K]
T_b	Air temperature at ground level [$^{\circ}C$]
T_{gnd}	Environmental ground surface temperature [K]
T_{sky}	Sky effective temperature [K]
T_{surf}	Surface outside face temperature [K]
u_i	Velocity component in the i -th direction [m/s]
u_j	Velocity component in the j -th direction [m/s]
u'	Root mean square of the velocity fluctuations
U_z	Local wind speed at height z above ground [m/s]
\vec{v}	Velocity vector [m/s]
W_f	Wind direction modifier

X_j	Response factor for the outside temperature at the j -th time step
Y_j	Response factor for the inside temperature at the j -th time step
Y	Dissipation of k due to turbulence [$kg/(m \cdot s^3)$]
z	Altitude [m]

Greek symbols

α	Wind velocity profile exponent
Γ	Effective diffusivity [m^2/s]
δ	Boundary layer thickness [m]
ε	Longwave emittance
ρ	Density [kg/m^3]
σ	Stefan-Boltzmann constant, equal to 5.67×10^{-8}
$\bar{\tau}$	Stress tensor [Pa]
ω	Specific dissipation rate [s^{-1}]

Abbreviations and acronyms

BC	Boundary conditions
BCVTB	Building controls virtual test bed
BES	Building energy simulation
BSD	Berkeley software distribution
CD	Computational domain
CFD	Computational fluid dynamic
CHTC	Convective heat transfer coefficients
CHTR	Convective heat transfer rate
CTBUH	Council on tall buildings and urban habitat
HVAC	Heating, ventilation, and air conditioning
HKW	Hong Kong winter period
HKS	Hong Kong summer period
LDW	London winter period
LDS	London summer period

NYW	New York winter period
NYS	New York summer period
RANS	Reynolds-averaged Navier-Stokes
SHGC	Solar heat gain coefficient
SHW	San Francisco winter period
SHS	San Francisco summer period
SFW	Shanghai winter period
SFS	Shanghai summer period
SST	Shear stress transport

1. Introduction

The heating and cooling of buildings are responsible for a significant portion of global energy consumption and carbon emissions, contributing to an environmental crisis in many societies [1]. The global popularity of high-rise buildings, along with climate changes, has prompted attention to the energy performance and environmental impact of these structures. A considerable portion of the energy demand for heating and cooling in the buildings can be attributed to the envelope heat loss/gain [2]. Notably, convective heat transfer on building façades plays an important role in determining the overall heat transfer through the building façades assembly [3]. Therefore, it is crucial to understand the influence of the wind environment on building external convective heat transfer coefficients (CHTC) and building energy performance.

Most building energy simulation (BES) programs utilize a nodal approach for heat transfer simulation and heating/cooling load calculations due to their computational efficiency and ease of implementation. However, this approach relies on various empirical coefficients, including the heat transfer coefficient [4]. Studies have shown that the CHTC used in BES can be prone to inaccuracies [4-8]. Different convection models employed to calculate the CHTC in BES have been shown to introduce errors in energy demand by up to 30% [9]. Emmel *et al.* [10] observed a 5% discrepancy in energy consumption when using accurate correlations. This suggests that relying on local air velocity as a key parameter for evaluating the CHTC may not be physically accurate. Instead, additional parameters that more accurately describe the airflow near the building envelope should be considered. High-rise buildings, with their unique surrounding wind environments and microclimate conditions at higher altitudes, may experience increased errors in predicting the energy performance of their envelopes.

One solution is to couple computational fluid dynamic (CFD) techniques with BES to achieve more accurate CHTC than using BES alone, due to the superior ability of CFD to model wind flows. On one hand, BES provides validated models for heating, ventilation and air conditioning (HVAC) systems and thermal load predictions and can supply dynamic boundary conditions (BC) to CFD. On the other hand, CFD offers more accurate CHTC values, which can enhance simulation results of energy demand in BES.

The coupling method can be classified into internal and external coupling based on how the models are solved. The internal coupling uses a single solver for both BES and CFD, while the external coupling uses separate solvers. Internal coupling requires researchers to access the source code of both simulators before implementation, making it impractical for commercial software [11]. In contrast, external

coupling provides the flexibility to customize each simulation separately and allows users to utilize each program without modifying the source codes.

The external coupling approach can be further classified based on the number and direction of data exchange. In static coupling, only one program provides data to the other throughout the entire simulation. Typically, microclimate results from CFD simulations are used to modify coefficient correlations or weather data in BES [7, 12-14]. In addition, some studies have employed parametric methods to investigate the CHTC correlation that can be used in BES, based on wind speed [15-17], and wind direction [18]. However, these correlations were found to be applicable only in specific scenarios.

Another method involves implementing a two-way coupling simulation scheme. In this dynamic coupling approach, data exchange between the two simulators occurs multiple times throughout the simulation. At each time step, data from one simulator is transferred to the other as boundary conditions to initialize the subsequent simulation. Data exchanged from BES to CFD include surface temperature, heat flux of the envelope, airflow rate, while data such as CHTC, airflow rate, humidity, etc., are returned to BES [4-6, 19-22]. In quasi-dynamic coupling, BES and CFD simulators solve their models individually, exchanging data at multiple time steps and then running simultaneously to the next step. Fully dynamic coupling requires iterations at each time step until both simulations converge. However, in studies utilizing this coupling method, certain meteorological variables, such as wind direction, were often oversimplified, considering only one [7] or several [4, 20, 23] specific wind directions.

1.1 Novelty, aims and objectives

Despite extensive research in this field, a significant gap remains in understanding the effects of modifications in exterior CHTCs on the convective heat transfer rate (CHTR), the balance of heat transfer at exterior surfaces, and the heating and cooling loads when employing coupling methods. Moreover, the effects of these changes on high-rise buildings, especially under diverse climatic conditions, have not been thoroughly examined. This study aims to address these gaps by focusing on multi-zone high-rise buildings under diverse climatic conditions. Using a coupling method between BES and CFD tools, we will explore how changes in exterior CHTCs affect the overall energy performance. This involves incorporating additional meteorological and microclimate data, with a particular emphasis on capturing detailed wind direction. A key aspect of our methodology includes the exchange of heat transfer information between the BES and CFD models at each timestep, facilitated by the Building Controls Virtual Test Bed (BCVTB) middleware and MATLAB scripts. Additionally, we will explore how different climatic conditions affect these relationships, making our study more robust and applicable to a wider range of scenarios.

We have modeled the high-rise building in various global cities, including London, Hong Kong, New York, San Francisco, and Shanghai, simulating a variety of climatic conditions. By systematically analyzing the impact of meteorological variables on CHTC values and assessing the variations in CHTC along the building height, the study aims to quantify the discrepancies between the proposed coupling method and algorithms used in BES, such as DOE-2, Simple Combined TARP, MoWiTT, and Adaptive Convection Algorithms. The overall goal is to provide data and insights that could lead to improvements in thermal performance strategies for different floors and specific building orientations, directly influencing the design, optimization, and energy conservation measures in high-rise buildings.

2. Literature review

Integrated models, combining CFD with BES, have gained prominence in the field of architectural engineering and environmental design. Their key role lies in providing a comprehensive analysis that bridges the complexities of airflow dynamics with building energy performance. While these models offer enhanced accuracy and detail, they also present challenges in terms of computational intensity and the complexity of coupling diverse simulation tools.

Many studies have been conducted to analyze CFD-BES integrated models to simulate geometrically complex buildings or natural, forced, or mixed convection analysis in buildings. Negrão [24] integrated a CFD code into the ESP-r building simulation program, this implemented an automated coupling method focused on an indoor space. Data, including the surface temperature of all the walls and windows, and the pressures at the internal openings, were exchanged on a timestep basis. This approach improved the simulation's accuracy by including crucial variables. Beausoleil-Morrison [25] then achieved a better description and simulation of the nature of the flow adjacent to each internal surface using a refined modelling approach and a conflation controller, resulting in a more comprehensive and accurate representation of the complex nature of indoor airflow. Based on these, other studies included experimental validation of the coupling method [26], research on the levels of resolution and complexity of the co-simulation [27], and the development of a coupling program and its interface [28].

As two methods of coupling BES and CFD tools, the application of internal coupling and external coupling were widely discussed [6, 11, 27]. The external coupling approach effectively addresses the limitations of internal coupling by using two independent and externally coupled simulators. Moreover, the external coupling provides greater flexibility and compatibility. The external coupling approach can be further classified into different coupling strategies according to the number and direction of data exchange: one-way static coupling, one-way dynamic coupling, two-way static coupling, quasi-dynamic coupling, and fully dynamic coupling. The features of these coupling strategies as well as the exchanged data between BES and CFD, were introduced and discussed by Zhai *et al.* [6]. The primary objectives of these strategies are to reduce computational expenses while preserving accuracy.

The one-way coupling strategies are used to investigate the impact of microclimate on the building [7, 12-14, 29-31]. In this case, the BES and CFD programs are manually coupled. Some of these studies replaced the weather data in EnergyPlus with the weather data modified according to the CFD results to represent a localized weather condition. The outputs of CFD can also be modified wind profile [29] and cross-ventilation rate [30]. Zhang and Gao [7] quantified the interaction between urban form, microclimate, and energy load for a residential district using the co-simulation method. The results show that the model simulated using modified microclimate data has a higher cooling demand and lower heating demand compared with the model simulated using the epw data, with the difference reaching 23.4%.

A similar approach is used by Yang *et al.* [12] and Weerasuriya *et al.* [13] to study the microclimate effects on building energy performance and natural ventilation potential, respectively. For instance, the coupling of ENVI-MET and EnergyPlus, considering a wide range of microclimatic factors such as solar and long-wave radiation, air temperature, humidity, and building surface wind speed, results in a 10.6% reduction in the total cooling load and a 0.3% increase in the total heating load [12]. Pan *et al.* [14] simulated the cooling load of atria in EnergyPlus based on different room air temperature patterns obtained from CFD simulation, the results were used to evaluate a simplified method of estimating cooling loads. It's noteworthy that while these investigations provided valuable insights into one-way coupling strategies, they did not explore the complexities of the CHTC. In contrast, subsequent studies shifted their focus to utilize local CHTC correlations derived from CFD, replacing the empirical model in BES and supplementing it with the modified weather data. Kahsay, *et al.* [31], [32] evaluated the energy consumption of a high-rise building by utilizing the newly developed CHTC derived from CFD results. An 8.53% deviation in heating and a 3.84% deviation in cooling for a building situated in Boston, MA was observed. However, only wind speed was considered in the CHTC correlations.

The CHTC is mainly studied when applying the two-way coupling strategies [4-6, 19-22]. Zhang *et al.* [4] compared the CHTCs and the air flow rate through openings simulated from the coupling model and nodal model using a quasi-dynamic coupling strategy, obvious differences in the CHTC values and the air flow rate were found. Zhai *et al.* [6] employed the two-way static coupling to investigate the cooling energy in an auto-racing complex, the prediction of cooling/heating load was improved due to the improvement in obtaining CHTCs in the coupling method. Yi and Feng [19] investigated the differences between CHTC from the coupling method and empirical model. Based on the co-simulation results, the values of CHTCs from CFD are 2-3 times larger than the empirical ones. Shen *et al.* [5],

Miguel *et al.* [20] and Zhang *et al.* [21] took the effect of urban neighborhoods into account in their analysis, finding that the coupling method better captures environmental influences on building energy consumption compared to empirical algorithms, which often underestimate heating loads. While the study of Gijón-Rivera *et al.* [22] focused on a room on top of a building and found that the coupling method generally provides higher accuracy in predicting air zone temperatures and cooling loads. The literature review highlights the role of integrated CFD and BES models in refining building energy simulations, enhancing our understanding of microclimatic impacts on energy efficiency in urban settings.

2.1 Research gaps

Despite extensive research in the field, there has been limited focus on the exterior Convective Heat Transfer Coefficients (CHTCs) for high-rise buildings. Shen *et al.* [5] studied the differences between EnergyPlus's built-in empirical methods and the coupling method for calculating exterior CHTCs, noting that CHTCs tend to increase with the building's height, influenced by high-altitude conditions. Additionally, few studies, such as Zhang, *et al.* [21], have incorporated wind direction into two-way coupling methods, using a cylindrical computational domain in a CFD model divided into 16 segments to capture wind direction variations at 22.5° intervals. Similarly, Shen and Wang [33] set specific boundary conditions for the simulation domain's four surfaces based on weather data files to account for varying wind directions. However, most studies primarily focus on the relationship between changes in exterior CHTCs and convective heat transfer rates (CHTR), as well as heating and cooling loads, with limited exploration of how modifications in CHTCs impact external surface temperatures and the overall heat transfer balance. This study aims to comprehensively investigate the effects of modifications in exterior CHTCs when employing a coupling method between BES and CFD tools, including the incorporation of additional meteorological and microclimate data with a specific focus on detailed wind direction. Our research also explores how modifications in exterior CHTCs impact CHTR, the balance of heat transfer at the external surfaces, and the heating and cooling loads when utilizing the coupling method.

3. Method

This section highlights the validation of the numerical model using empirical measurements made in a wind tunnel, a description of the coupling method between BES and CFD, and BES and CFD models used for the coupling method. The validated CFD model has been used to investigate the effect of meteorology variables on convective heat transfer coefficients and the energy demand of high-rise buildings with multi-thermal zones.

3.1 Numerical model validation with experimental data

The validation of CFD refers to the wind tunnel experimental results by Meinders *et al.* [34] and the CFD simulation of typical high-rise building models. The experiment was carried out to investigate the convection heat transfer at the surfaces of a heated cube, where the cube was placed in turbulent channel flow. As shown in Figure 1(a), the height of the channel is 0.05 m, and the width is 0.6 m. The cube contains a copper core and an epoxy layer, and the height of the cube is $H_c = 0.015$ m, as shown in Figure 1(b). The copper core had high thermal conductivity and was heated at a constant temperature of 348 K (75 °C). The Epoxy has a density of $1,191 \text{ kg/m}^3$ and a specific heat capacity of $1,650 \text{ J/kg}\cdot\text{K}$. The thermal conductivity of the epoxy layer is $0.237 \text{ W/m}\cdot\text{K}$. Temperature distribution on the surface of the cube was measured. The experiments were performed using a perpendicular approach flow, and relatively low Reynolds numbers ranged from 2000 to 5000. The free stream velocity was 5.1 m/s, and the velocity profile is shown in Figure 1(d). The inlet air temperature is 294 K (21 °C). These profiles fit into a log-law with aerodynamic roughness length $z_0 = 6.6 \times 10^{-6} \text{ m}$ and a friction velocity $u^* = 0.25 \text{ m/s}$. The exterior surfaces of the cube are defined as no-slip boundaries with zero roughness. For the ground boundary of the domain, no-slip boundary conditions and an adiabatic surface are assumed. Zero static pressure is applied at the outlet, and symmetry boundary conditions are specified

at the top and sides of the computational domain (CD). Details of the experiments can be found in Meinders *et al.* [34].

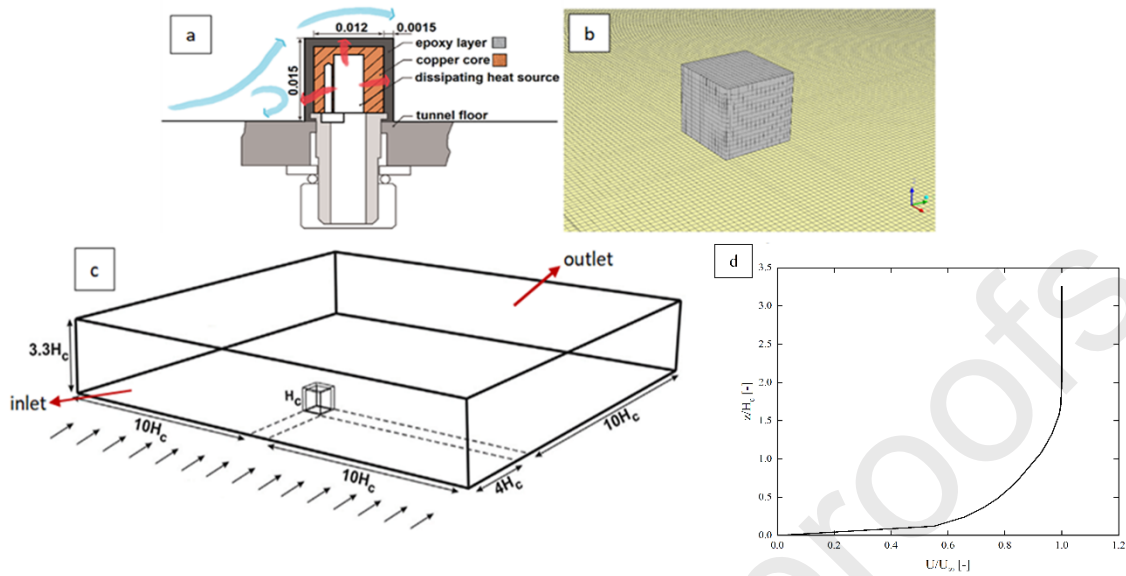


Figure 1 Experimental setup of Meinders *et al.* [34]: (a) cross-section of the heated cube, (b) meshed model, (c) three-dimensional view of the experiment channel and (d) inlet velocity profile.

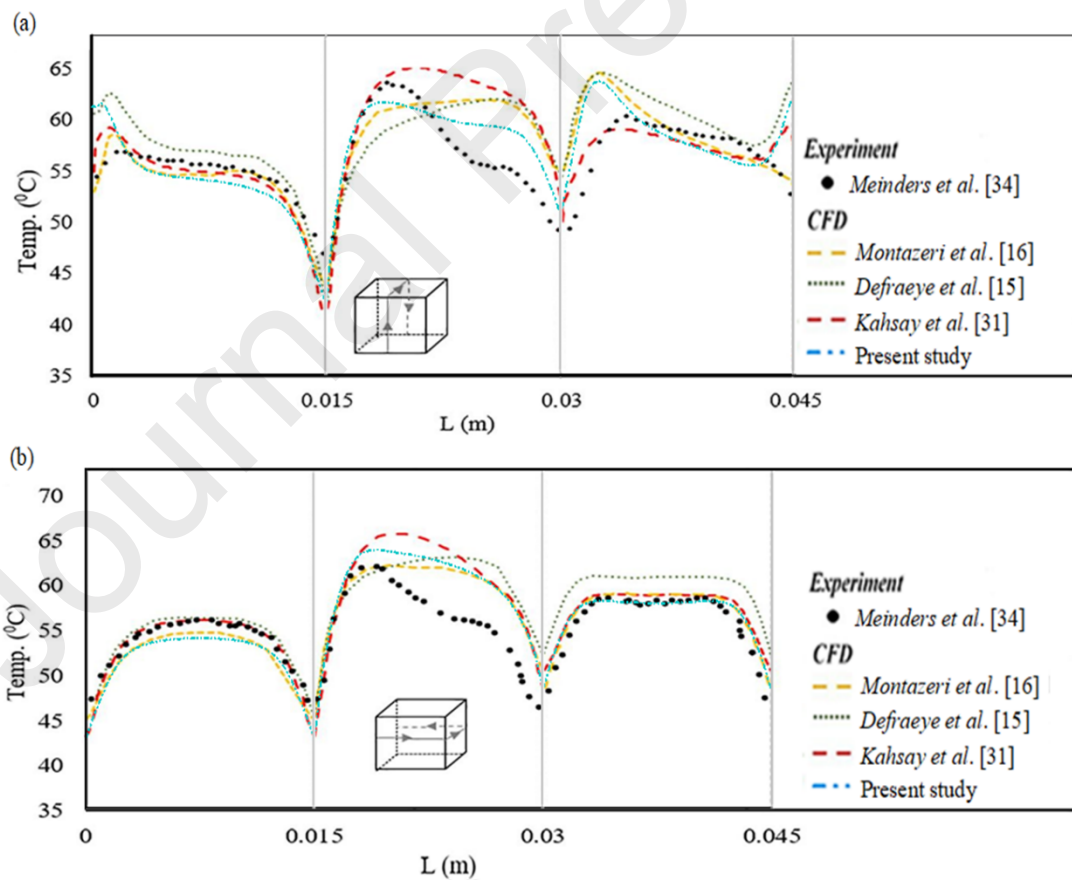


Figure 2 Comparison of simulated temperature distribution along (a) vertical and (b) horizontal lines on the middle of the cube surfaces with experiment and previous study simulations.

The numerical model for the validation is based on the experiment [34] and previous validation work by Montazeri *et al.* [16], Defraeye *et al.* [15] and Kahsay *et al.* [31], including computational domain, boundary conditions, and solver settings. The maximum grid distance is 2.94×10^{-6} m from the cube surfaces, resulting in a maximum y^+ value of 0.20 over the cube surfaces. The validation simulation only considered forced convection as the relative importance of buoyancy effects is assumed negligible [16]. Temperature distributions along horizontal and vertical middle lines on the surface of the cube were measured. These values were compared with the simulated temperature values using the *shear stress transport $k-\omega$* (*SST $k-\omega$*) model shown in Figure 2.

In comparison, even with a relatively larger deviation along both the vertical and horizontal lines on the windward surface than in previous studies [16, 31], the average deviations are less than 6%. For the side and leeward surfaces, the *SST $k-\omega$* model overestimated the temperature, typically in the top, mid-rear on the side surfaces, and upper on the leeward surface. This overestimation is primarily due to the inaccurate flow field prediction by the 3D steady Reynolds-averaged Navier-Stokes (RANS) models downstream of the windward façade [18]. Such discrepancies in flow field predictions contribute to lower CHTC values at these surfaces, which could affect energy performance predictions.

Our observations are consistent with findings from previous studies by Montazeri *et al.* [16], Defraeye *et al.* [15] and Kahsay *et al.* [31]. The airflow dynamics around the top and side surfaces are typically more complex due to factors such as boundary layer separation and flow reattachment on the top surfaces. Similarly, side surfaces are often subjected to crosswind effects that introduce three-dimensional turbulence effects, complicating the airflow patterns. These complexities make it challenging for CFD models to accurately simulate the flow and predict heat transfer rates along these surfaces. Furthermore, when considering the model of the high-rise building, the top surface constitutes a relatively small portion of the total building surface area, limiting the scope of impact from temperature estimation errors. Conversely, the building's sides, which cover a larger area, could be more affected by these inaccuracies. Therefore, careful consideration is necessary for these areas during simulations, as errors here substantially influence the overall energy predictions of the building. Overall, the *SST $k-\omega$* model results showed good consistency in temperature trends hence, it is used in the CFD simulation in this study.

3.2 Approach of the coupling method

The schematic of the coupling process for this study is presented in Figure 3. This study adopts external coupling, where separate solvers are used for BES and CFD software, with EnergyPlus used as the BES tool and ANSYS Fluent as the CFD program. Quasi-dynamic coupling is adopted due to the requirements for multiple data exchanges. Among different dynamic coupling strategies, quasi-dynamic coupling offers a balance between accuracy and speed. A consistent geometry is created in both BES and CFD, and a total of 18 CFD models were developed to simulate different wind directions. Details of the BES and CFD modeling are provided in later sections.

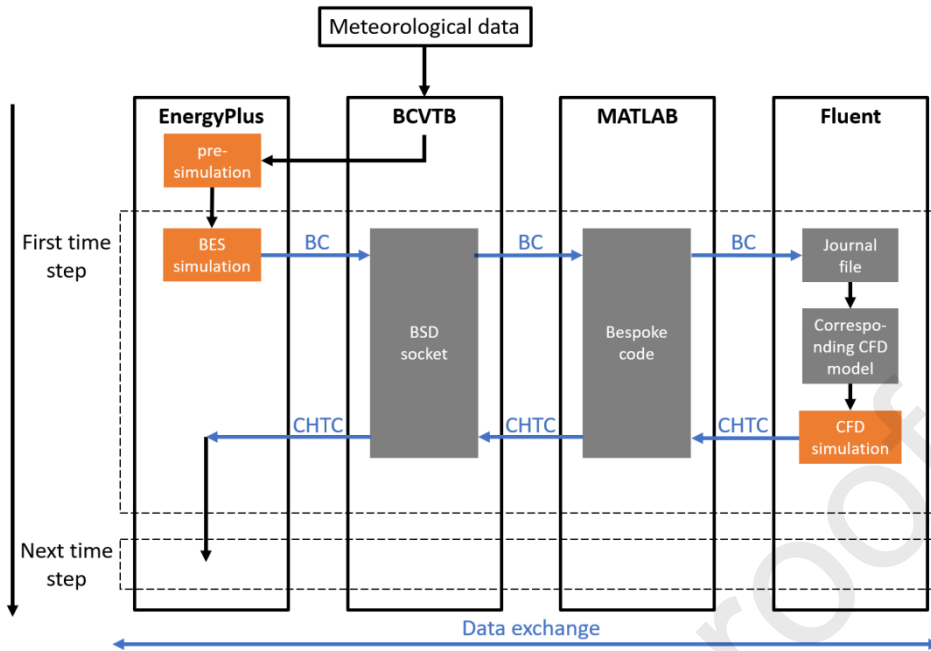


Figure 3 The schematic of the coupling process between FLUENT, MATLAB and BCVTB and EnergyPlus.

The integration between EnergyPlus and ANSYS Fluent is implemented through the Building Controls Virtual Test Bed (BCVTB) [35]. BCVTB is a software environment based on Ptolemy II, used to couple several simulation software programs. Data is transferred between these programs using a BSD socket. However, since BCVTB cannot directly couple with Fluent, MATLAB is used to connect BCVTB and Fluent. A bespoke code in MATLAB was developed to transfer data from BES into a journal file format, which is used to set the boundary conditions and start calculations in CFD for each time step. It also selects the corresponding CFD model based on the wind direction for the present time step.

A text-based variable configuration file named "variable.cfg" contains all the variables to be exchanged during the co-simulation. CFD requires meteorological data and building surface temperatures as boundary conditions. The meteorological data includes wind speed, wind direction, and air dry-bulb temperature, all obtained from the epw weather data file. Area-average exterior CHTCs for building surfaces are calculated by CFD and then transferred back to BES. An ExternalInterface: Actuator was added to replace the exterior CHTC values with CFD results during the co-simulation in EnergyPlus. EnergyPlus runs for two days before coupling to establish initial conditions.

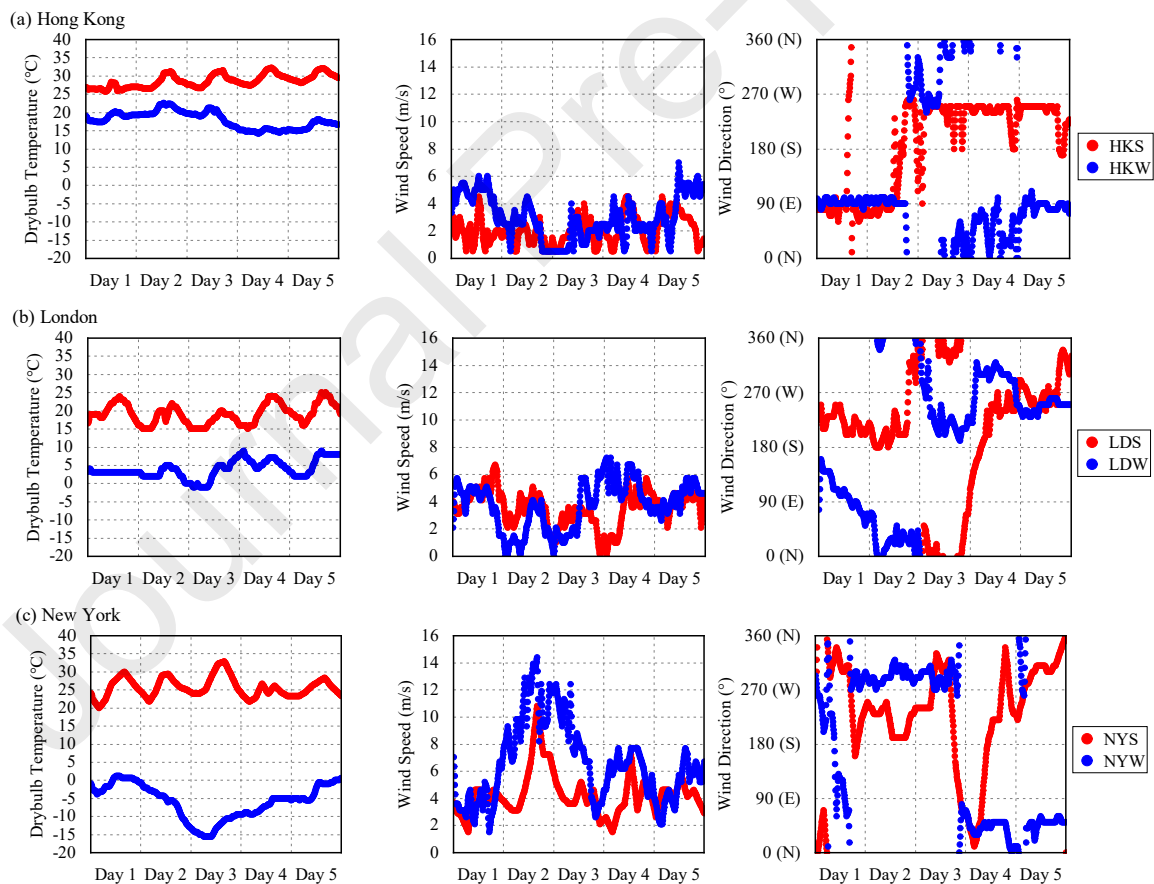
Due to the mechanism of Ptolemy II, the variables are exchanged between BES and CFD using a fixed synchronization time step. At time point k , the meteorology data and surface temperatures are transferred from BES to CFD as boundary conditions. CFD then runs a steady-state simulation for the present time step. After calculation, CFD returns exterior CHTCs at time point k to BES as boundary conditions for energy simulation at time point $k+1$. Initially, in EnergyPlus, CHTCs can be set either directly for surfaces by providing input for the respective surfaces in the EnergyPlus model or indirectly through the definition of constructions for building surfaces.

In comparison with BES alone, using this quasi-dynamic coupling has a one-time step interval difference regarding the convective heat transfer calculation to the building envelopes. Therefore, the length of the time step for the coupling method is selected with certain requirements. For this study, a time step of 10 minutes is selected as recommended [6, 19, 36]. This means EnergyPlus and Fluent will simulate 6 times per hour, accounting for a total of 720 simulations per simulation period.

The quasi-dynamic coupling strategy used in this study captures the dynamic variations in environmental conditions and their immediate effects on convective heat transfer coefficients (CHTC) throughout the selected 5-day simulation periods. This approach allows us to incorporate the temporal changes in local weather and building surface conditions as dynamic boundary inputs, providing a more detailed understanding of CHTC behaviors under realistic, fluctuating climatic conditions. Although this coupling strategy does not require iteration between BES and CFD to reduce computational times, it remains computationally intensive for seasonal or yearly simulations. Each 5-day simulation period requires approximately 240 hours of computational time on a computer equipped with an AMD Ryzen 7 3700X 8-Core Processor running at a clock speed of 3.60 GHz and 32GB of memory.

3.3 Simulation locations and weather data

A summer period of five days (July 21st to 25th) and a winter period of five days (January 21st to 25th) were chosen for the evaluation. The co-simulation considered a high-rise building located in five different cities with varying climate conditions during the selected simulation periods: London (LD), Hong Kong (HK), New York (NY), San Francisco (SF), and Shanghai (SH). These cities have a high number of high-rise buildings and high population densities, indicating a continued demand for constructing high-rise buildings in the future, according to the Council on Tall Buildings and Urban Habitat (CTBUH) [37]. Figure 4 presents the weather data for air dry bulb temperature ($^{\circ}\text{C}$), wind speed (m/s), and wind direction ($^{\circ}$) for the selected locations during the selected summer and winter simulation periods. These figures represent typical weather conditions for each location and demonstrate various combinations of wind patterns, with both wind speed and direction exhibiting significant variations.



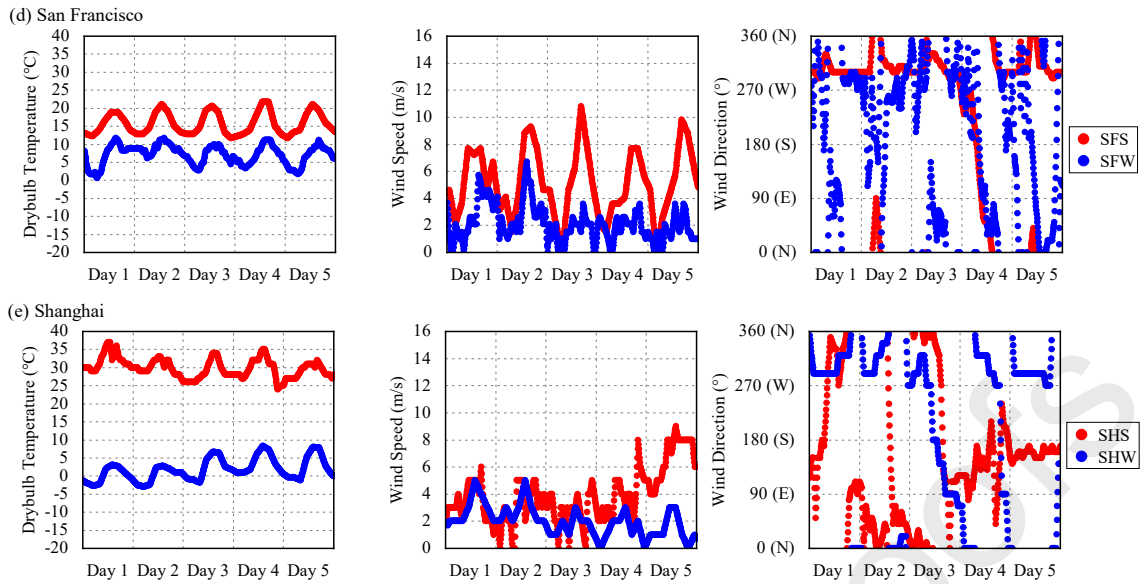


Figure 4 Weather data of air dry bulb temperature, wind speed, and wind direction during the summer and winter periods in (a) Hong Kong, (b) London, (c) New York, (d) San Francisco, and (e) Shanghai.

3.4 BES modelling

The energy model of the building (see Figure 5) is based on a medium office developed by the Department of Energy [38], incorporating the configuration of the envelope, its materials, densities of internal heat gains from different sources, and their profiles. Each story is considered a thermal zone. The building has 36 floors, each with a height of 3.96 m, and a basement with a height of 2.44 m, giving a total height of 142.56 m above the ground. The length and width of the building are 73.11 m and 48.74 m, respectively.

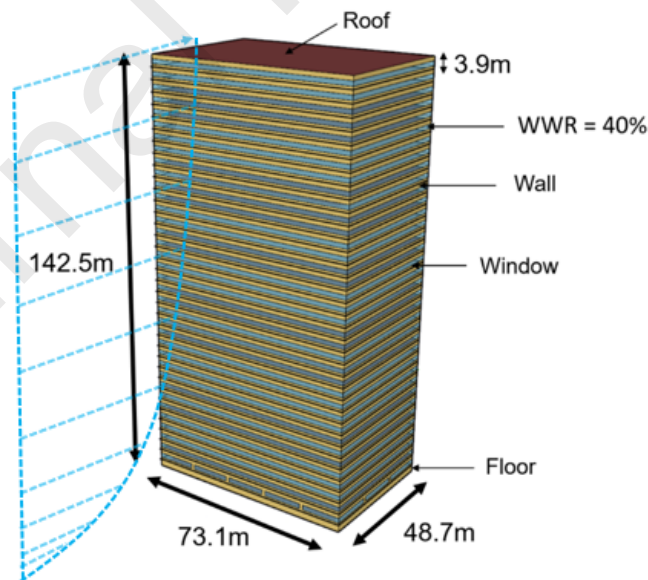


Figure 5 The energy model of the high-rise building based on the US Department of Energy commercial reference building models of the national building stock.

The building is occupied as an open-plan office for 70% of its area. Each floor, except for the ground floor and the basement, has four windows located in the middle of each oriented façade. The window-to-wall ratio was set at 40% for all surfaces. The windows have a height of 1.59 m, with an elevation

of 0.91 m from the floor level. On the ground floor, the windows are 1.7 m in height, with an elevation of 0.80 m from the floor level. The windows on the ground floor have two different widths, 13.65 m and 15.43 m, depending on the oriented façade. The basement has no windows.

There is no natural ventilation for the building, and there is no shade control for the windows; hence, the analysis will be fully based on wall fabric heat transfer. Exterior heat transfer coefficients calculated using various convection models in the BES model will be compared with those calculated using the coupling method.

This high-rise building is occupied between 7 am and 10 pm on weekdays. The occupancy percentage is 10% at 7 am and 20% at 8 am. It increases to 95% at 9 am and is fully occupied between 11 am and 1 pm. During the lunch break from 1 pm to 2 pm, occupancy decreases to 50%. From 2 pm to 5 pm, the occupancy returns to 95%. After 6 pm, occupants start to leave, with the percentage dropping to 30%, and further to 10% at 7 pm until 10 pm. The internal gains for people, lighting, and equipment are 6.45 W/m², 6.89 W/m², and 7.77 W/m² for occupied areas, respectively.

Other configurations of the energy model, such as U-values and temperature thresholds for heating and cooling when occupied, for the high-rise building located in each city, are listed in Table 1. U-values are set according to the local benchmark for new commercial buildings [39, 40], representing high standards of thermal performance for building façades. The operative temperature is maintained between 15.6°C and 26.7°C during unoccupied hours, while the building space is heated to 21°C during the winter period and cooled to 24°C during the summer period. An ideal air system load was used for simplification. The solar heat gain coefficient (SHGC) of the windows is 0.251 for all locations.

Table 1 Energy model building *U-values* based on [39]

<i>U-values (W/m²K)</i>				
	External roof	External wall	Floor	Glazing
London	0.21	0.592	0.496	2.27
Hong Kong	0.21	0.701	0.606	3.69
Shanghai	0.21	0.857	0.606	4.26
New York	0.21	0.592	0.496	2.27
San Francisco	0.21	0.701	0.606	3.69

Verification of the BES modelling approach based on the EnergyPlus building model was carried out in previous works, for example [41]. The outside surface heat balance in EnergyPlus is calculated as [42]:

$$q''_{\text{asol}} + q''_{LWR} + q''_{\text{conv}} - q''_{ko} = (1)$$

where q''_{asol} is the absorbed direct and diffuse solar radiation heat flux, influenced by location, surface facing angle and tilt, surface face material properties, and weather conditions. q''_{LWR} is the net longwave radiation flux exchange with the air and surroundings. q''_{conv} is the convection flux exchange with outside air, and q''_{ko} is the conduction heat flux into the wall.

The total longwave radiative heat flux, q''_{LWR} , is calculated by the sum of components due to radiation exchange with the ground, sky, and air:

$$q''_{LWR} = \varepsilon\sigma F_{gnd}(T_{gnd}^4 - T_{surf}^4) + \varepsilon\sigma F_{sky}(T_{sky}^4 - T_{surf}^4) + \varepsilon\sigma F_{air}(T_{air}^4 - T_{surf}^4) \quad (2)$$

where ε is the longwave emittance of the surface, σ is Stefan-Boltzmann constant, F_{gnd} , F_{sky} , and F_{air} are view factor of wall surface to ground surface, sky, and air, respectively, T_{surf} , T_{gnd} , T_{sky} , and T_{air} are the temperature of the outside surface, ground surface, sky, and outside air, respectively. The ASHRAE Clear Sky Model is employed in present study for calculating T_{sky} across all locations, utilizing input variables such as dry bulb temperature, dew point temperature, direct normal radiation, diffuse horizontal radiation, and sky cover, sourced from the epw weather files specific to each location. Additionally, solar positions were calculated using the latitude, longitude, and elevation specified in the Site: Location object for each site.

The exterior convection flux, q''_{conv} , is calculated by:

$$q''_{\text{conv}} = h_{c,ext}A(T_{surf} - T_{air}) \quad (3)$$

where $h_{c,ext}$ is exterior convection heat transfer coefficient (CHTC), and A is surface area.

The conduction heat flux at the outside surface at current time step t , $q''_{ko}(t)$, is calculated using the Conduction Transfer Function (CTF) method:

$$q''_{ko}(t) = \sum_{j=0}^{\infty} X_j T_{o,t-j\delta} - \sum_{j=0}^{\infty} Y_j T_{i,t-j\delta} \quad (4)$$

where T is temperature, i and o signify the inside and outside of the building element, respectively, X_j and Y_j are the response factors for the outside and inside temperatures, respectively. The term $t - j\delta$ denotes the temperature at time t minus j intervals of δ .

3.4.1 Exterior Convection

The values for CHTC can be determined by a wide selection of different methods in EnergyPlus, including the DOE-2 model, Simple Combined, TARP, MoWiTT, and adaptive convection algorithm [42]. The DOE-2 model, which is the default model used in EnergyPlus to calculate the exterior convection heat transfer coefficient, is one of the most widely utilized models for estimating building energy performance. Detailed comparisons of the changes in CHTC, CHTR, and wall heat balance with the coupling method in the results section are based on the DOE-2 model.

The DOE-2 model combines the MoWiTT and BLAST detailed convection models, considering whether the surface is windward or leeward and its surface roughness [43]. The equations are written as follows:

$$h_{c,ext} = h_n + R_f(h_{c,glass} - h_n) \quad (5)$$

$$h_{c,gl\text{ass}} = \sqrt{h_n^2 + [aU_z^b]^2} \quad (6)$$

where h_n is natural convective heat transfer coefficient, R_f is surface roughness multiplier, $h_{c,gl\text{ass}}$ is the convection coefficient for smooth surfaces such as glass, a and b are MoWiTT coefficients, and U_z is the local wind speed calculated at the height above ground of the surface centroid.

Additionally, we conducted and presented comparative studies involving the Simple Combined, MoWiTT, TARP, and Adaptive Convection Algorithms. This includes the comparison of CHTC and CHTR along the building height and the heating/cooling demand between these algorithms and the coupling method.

The Simple Combined algorithm calculates a combined convection and radiation heat transfer coefficient, h , uses surface roughness and local surface wind speed [44]:

$$h = D + EU_z + FU_z^2 \quad (7)$$

where D, E and F are material roughness coefficients.

The TARP (Thermal Analysis Research Program) algorithm calculates forced (h_f) and natural (h_n) convection as two components of the convection heat transfer coefficient [45]:

$$h_{c,ext} = h_f + h_n \quad (8)$$

The forced convection component is calculated by [46]:

$$h_f = 2.537W_f R_f \left(\frac{PU_z}{A} \right)^{1/2} \quad (9)$$

where the value of W_f is 1.0 or 0.5, corresponding to windward or leeward surfaces, respectively, and P is the perimeter of surface.

The natural convection component for a vertical surface is calculated based on the temperature difference between the surface and air, ΔT :

$$h_n = 1.31|\Delta T|^{1/3}$$

The MoWiTT (Mobile Window Thermal Test) model [47] calculates the $h_{c,ext}$ by:

$$h_{c,ext} = \sqrt{\left[C_t(\Delta T)^{1/3} \right]^2 + [aU_z^b]^2} \quad (11)$$

where C_t is the turbulent natural convection constant with a value of $0.84 \text{ W}/(\text{m}^2\text{K}^{4/3})$, while a and b are constants depending on whether the surface is windward or leeward.

The Adaptive Convection Algorithm for exterior surfaces is composed of separately developed correlations to calculate forced and natural convection. EnergyPlus dynamically selects these correlations based on surface conditions. The algorithm classifies surfaces into four categories: stable roof, unstable roof, windward vertical wall, and leeward vertical wall, depending on the current wind direction and heat flow directions.

3.5 CFD modeling

The CFD modelling was performed using the *SST k- ω* turbulence model was used, and all the equations were solved by the COUPLE algorithm. The general form of the continuity equation is written as follows [48]:

$$\frac{\partial \rho}{\partial t} + \nabla \cdot (\rho \vec{v}) = S_m \quad (12)$$

where ρ is the density, \vec{v} is the velocity vector, and S_m is the user-defined mass sources.

The momentum conservation equation is described by:

$$\frac{\partial}{\partial t}(\rho \vec{v}) + \nabla \cdot (\rho \vec{v} \vec{v}) = -\nabla p + \nabla \cdot (\bar{\tau}) + \vec{F}_b \quad (13)$$

where p is the static pressure, $\bar{\tau}$ is the stress tensor, and \vec{F}_b is the body forces.

The energy equation is solved in Fluent by:

$$\frac{\partial}{\partial t}(\rho E_{total}) + \nabla \cdot (\vec{v}(\rho E_{total} + p)) = \nabla \cdot \left(k_{eff} \nabla T - \sum_j h_j \vec{J}_j + (\bar{\tau}_{eff} \cdot \vec{v}) \right) + S_h \quad (14)$$

where k_{eff} is the effective conductivity, \vec{J}_j is the diffusion flux of species j . The terms on the right hand side of the energy equation represent energy transfer due to conduction, species diffusion, viscous dissipation, and user-defined heat sources (S_h), respectively. In the present study, the species diffusion and user-defined heat source terms were set to zero.

The transport equations for the *SST k- ω* model are [49]:

$$\frac{\partial}{\partial t}(\rho k) + \frac{\partial}{\partial x_i}(\rho k u_i) = \frac{\partial}{\partial x_j} \left(\Gamma_k \frac{\partial k}{\partial x_j} \right) + \tilde{G}_k - Y_k + S_k \quad (15)$$

$$\frac{\partial}{\partial t}(\rho \omega) + \frac{\partial}{\partial x_j}(\rho \omega u_j) = \frac{\partial}{\partial x_j} \left(\Gamma_\omega \frac{\partial \omega}{\partial x_j} \right) + G_\omega - Y_\omega + D_\omega + S_\omega \quad (16)$$

where \tilde{G}_k represents the generation of turbulence kinetic energy due to mean velocity gradients, G_ω represents the generation of ω . Γ_k and Γ_ω represent the effective diffusivity of k and ω , respectively, Y_k and Y_ω represent the dissipation of k and ω due to turbulence, D_ω represents the cross-diffusion term, and S_k and S_ω are the source terms. The extra cross diffusion term D_ω is the blending function for the standard k - ϵ model and standard k - ω model.

The CFD model was built according to the EnergyPlus model with the same geometry setup and is based on previous studies with a similar approach [15-17]. As shown in Figure 6(a), the size of the CD is set with respect to the height of the high-rise building, represented by $H = 142.56$ m. According to the recommendations of Tominaga *et al.* [50], the distance from the top of the building to the top of CD is set as $3.3H$, with an upstream length of $5H$, a downstream length of $15H$ and a side distance of $5H$ from the high-rise building.

A grid independency analysis is conducted for the *SST k- ω* model with coarse (1,463,678 cells), medium (4,244,866 cells) and fine (8,478,174 cells) grids. Figure 6(b) shows the results of the grid independence analysis based on the exterior CHTC along the building surfaces. The average difference in percentage between the coarse and medium grids is 4.7%, while the average difference in percentage between the medium and fine grids is 1.8%. The result does not change significantly between the medium and fine grid, and the medium grid is therefore used in this study for the CFD simulations. Polyhedron-

hexahedron cells were used for computational efficiency. A refined grid region near the building surfaces and a boundary layer of 10 prism layers were applied on the building surfaces with a stretching factor of 1.05 to achieve small y^+ values.

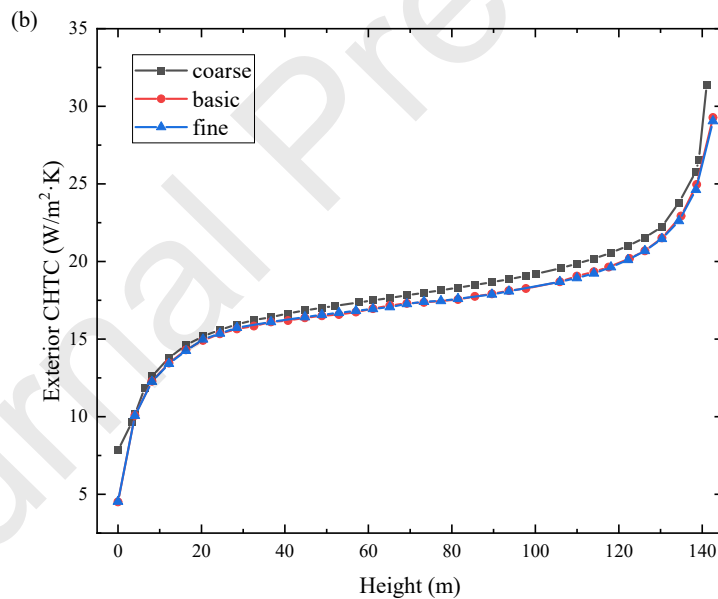
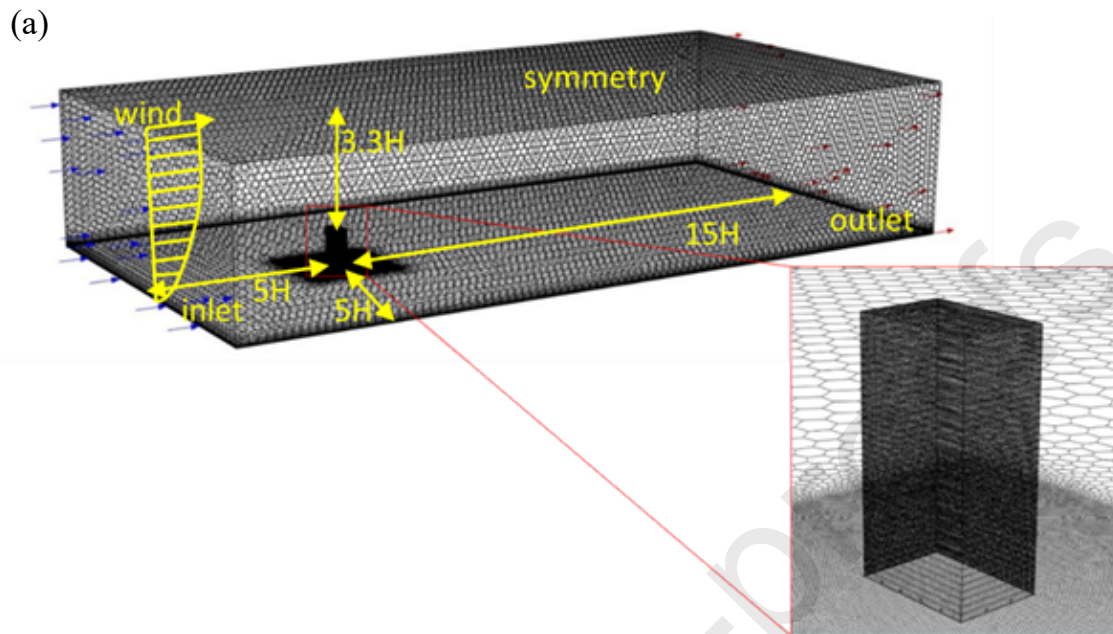


Figure 6 (a) The dimension of the computational domain, boundary conditions and mesh design (b) Grid independency analysis based on the exterior CHTC across the building height.

During each time step, the bespoke MATLAB code reads wind direction information through the BSD socket in BCVTB. For different wind directions, the bespoke code specifies the corresponding CFD model in the journal file when generating it and applies the boundary condition (BC) information for the four differently oriented façades to the corresponding surfaces in the CFD model. Convergence was achieved when all the scaled residuals leveled off and reached a minimum of 10^{-6} for energy, x, y, and z momentum, and 10^{-4} for continuity, k, and omega.

By rotating this CFD model around the center of the building geometry in multiples of 10 degrees, a total of 18 CFD models were created to simulate the impact of different wind directions. Each model can represent two wind directions by assigning different boundary conditions to the surfaces. Except for the angle of the building's windward façade from the inlet airflow, which changes due to the rotation, the setup of the CFD models, including grid settings, CD, and BC, remains the same. The total grid number of these 18 models has minor differences due to the rotation of the building geometry. In this way, 18 models can be used to simulate 36 wind directions to achieve the same wind direction as recorded in the weather data file.

It should be noted that although there are only 36 wind directions in multiples of 10 degrees in the epw weather data file, EnergyPlus will linearly adjust the wind direction of each time step according to the hourly weather data. Therefore, each time step can have a wind direction that is not a multiple of 10 degrees. In this case, the bespoke MATLAB code will select the CFD model that is closest to the current wind direction at each time step.

3.5.1 Boundary conditions of CFD domain

For each time step, the ground is set as a no-slip wall with a constant temperature derived from the epw weather data, and symmetry boundary conditions are applied at the top and lateral sides of the computational domain (CD). The outlet is a pressure outlet with zero static pressure. The temperature of the walls and ground is set directly in the journal file, and the boundary conditions for the inlet are set using Fluent expressions in the journal file. The use of Fluent expressions reduces the computational time required to compile and load user-defined functions (UDFs).

For the inlet boundary conditions, the airflow properties are set using the same algorithm as EnergyPlus. For the inlet boundary conditions, the airflow properties are set to be the same algorithm used in EnergyPlus. Based on the EnergyPlus engineering reference [42], local wind speed, U_z , at altitude, z , can be calculated by:

$$U_z = U_{met} \left(\frac{\delta_{met}}{z_{met}} \right)^{\alpha_{met}} \left(\frac{z}{\delta} \right)^{\alpha} \quad (17)$$

where α is the wind velocity profile exponent and δ is the boundary layer thickness at the site, both parameters depend on the roughness characteristics of the local terrain. The subscript 'met' refers to the data collected at the meteorological station. The default value for z_{met} is 10 m for wind speed measurement. The default values for α_{met} and δ_{met} are 0.33 and 460 m in a typical city terrain.

The relationship between air temperature, T_z (°C), and altitude is calculated by:

$$T_z = T_b + L \left(\frac{Ez}{(E+z)} - H_b \right) \quad (18)$$

where L is the air temperature gradient with the value of -0.0065 K/m, E_r is the radius of the Earth with the value of 6,356 km, and T_b (°C) is air temperature at ground level, since it refers to the air temperature at ground level, it can be calculated by:

$$T_b = T_{z_{met}} + L \left(\frac{E_r z_{met}}{(E_r + z_{met})} \right) \quad (19)$$

where $T_{z_{met}}$ (°C) is the air temperature in the weather file, z_{met} is the height above the ground of the air temperature sensor at the meteorological station with a default value of 1.5 m.

In addition to the meteorology variables used in EnergyPlus, there are two additional inlet boundary profiles used in CFD, which are local turbulence kinetic energy, k_z , and the turbulence dissipation rate, ε_z , at altitude z . They can be calculated as below [51]:

$$k_z = \frac{u'_{u,z}{}^2 + u'_{v,z}{}^2 + u'_{w,z}{}^2}{2} \cong \frac{3}{2} u'_z{}^2 = \frac{3}{2} (I_z U_z)^2 \quad (20)$$

where u'_z is the local root mean square of the velocity fluctuations in the stream-wise direction and I_z is the local turbulent intensity that can be calculated by:

$$I_z = \frac{u'_z}{U_z} = 0.1 \left(\frac{z}{\delta} \right)^{-\alpha-0.05}$$

$$\varepsilon_z = C_\mu^{1/2} k_z \frac{U_{ref}}{z_{ref}} \alpha \left(\frac{z}{z_{ref}} \right)^{\alpha-1} \quad (22)$$

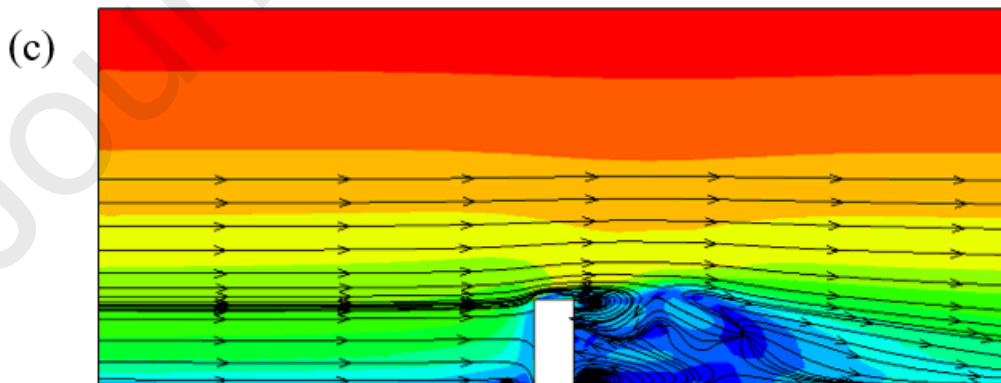
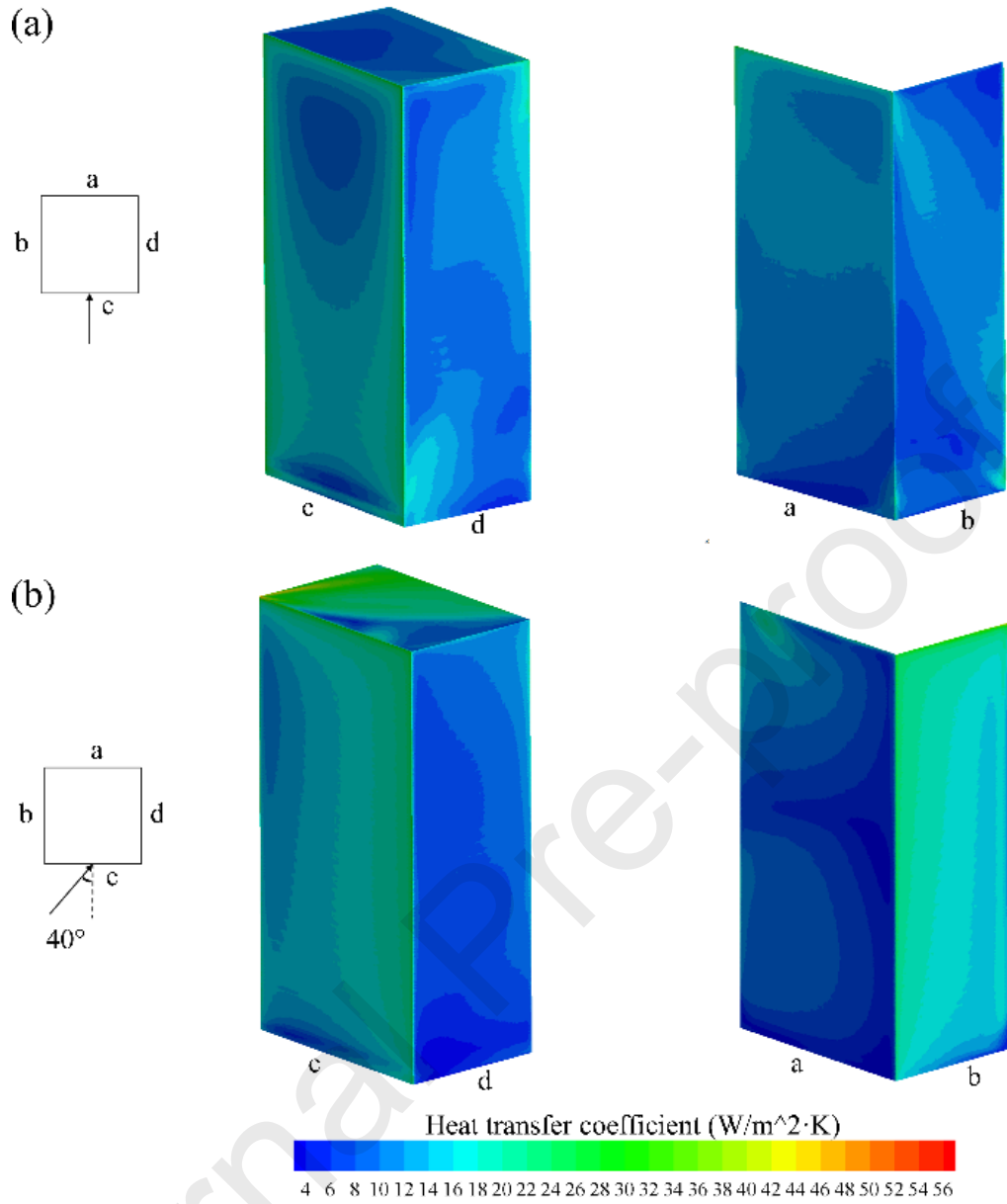
where C_μ is a constant with a value of 0.09, U_{ref} and z_{ref} are reference wind speed and local height and are set as meteorological data U_{met} and z_{met} , respectively.

4. Results and Discussion

4.1 Impact of wind pattern on exterior CHTC

The variation of the exterior CHTC along the building height, as influenced by wind patterns, presents a detailed perspective on façade-specific energy performance. According to the findings illustrated in Figure 6, different windward and leeward façades respond uniquely to wind directions and speeds, highlighting the complexity of airflow dynamics around high-rise structures.

The data from Figures 7(a) and 7(b) show that at wind speeds of 3 m/s, measured 10 m above ground, the distribution of CHTC exhibits significant spatial variability influenced by wind direction. Specifically, when wind approaches 0° , higher CHTC values are predominantly found on the windward side, indicative of more direct wind impact and enhanced convective heat transfer. However, the top and bottom sections of the building and its boundaries show marked decreases in CHTC values, possibly due to turbulence and flow separation effects that reduce wind speed in these regions, thereby decreasing convective heat removal. The CHTC on the leeward side shows a general increase from bottom to top. This phenomenon could be attributed to complex airflow patterns, including vortex shedding and recirculation. The higher CHTC at the top of the leeward side might result from increased turbulence and mixing, driven by wind flow over the building's crest.



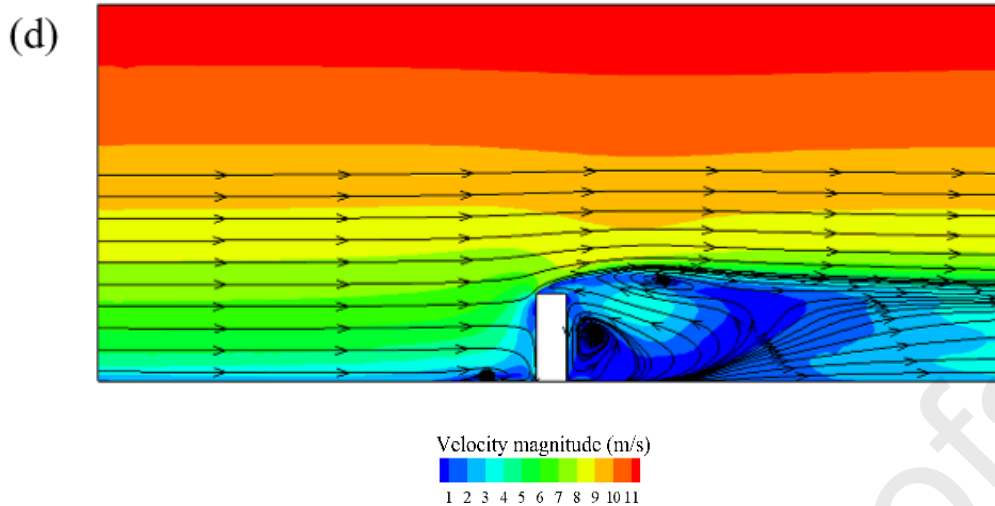


Figure 7 CHTC contours for wind direction of (a) 0° and (b) 40° and velocity contours for wind direction of (c) 0° and (d) 40° when the wind speeds are 3 m/s at 10 m above ground.

When the wind direction shifts to 45° , the asymmetry in wind exposure becomes more pronounced, particularly affecting the CHTC distribution along the building's edges. The right edge of the windward façade and the opposing left side exhibit higher CHTCs due to altered airflow paths, emphasizing the significance of building orientation relative to prevailing wind directions. This observation suggests that for accurate thermal modeling, the angular incidence of wind on façades must be taken into account, extending beyond the traditional binary categorization into windward and leeward sides.

These findings highlight a gap in conventional BES tools, which often simplify wind impacts based on generic windward and leeward definitions without accounting for angular variations and specific local wind conditions. Consequently, this can lead to inaccuracies in predicting thermal loads and energy performance, particularly in the design and optimization of high-rise buildings in urban environments.

Furthermore, the variations in wind patterns around the building, as depicted in Figures 7(c) and (d) can be correlated with the exterior CHTC patterns observed under varying wind directions. This indicates the necessity for dynamic modeling approaches that can account for wind effects and detailed façade orientations. The current study emphasizes the relationship between localized airflow patterns and convective heat transfer, suggesting that future research should aim to integrate more granular wind data and detailed geometrical modeling into energy simulation tools for better prediction accuracy.

Figure 8 shows the average exterior CHTC for differently oriented façades, calculated using (a) the coupling method and (b) the DOE-2 algorithm, plotted against wind speed at a height of 10 m for each time step across the five cities. The wind speeds are based on the weather data in the epw file. The simulations for both the summer and the winter periods in the five cities result in a comprehensive dataset of 7200 values, corresponding to each time step. Figure 8(c) presents the differences between these two approaches for each time step. Both the coupling method and the DOE-2 algorithm reveal distinct windward and leeward characteristics. A robust correlation between the average CHTC values and wind speed can be observed in both approaches, indicating the dominant influence of wind speed on the exterior CHTC. However, the coupling method introduces variations in CHTC values under specific wind speed conditions due to the consideration of wind directions. In contrast, results from the DOE-2 algorithm are more concentrated, lacking a significant correlation with wind directions.

Upon comparison, the CHTC values for the leeward façades show minimal differences between the two approaches, whereas the windward façades exhibit substantial variations. The coupling method calculates higher CHTC values than the DOE-2 algorithm for windward façades, with a maximum difference of $53.69 \text{ W/m}^2 \cdot \text{K}$. Meanwhile, the CHTC values of the leeward façades calculated using the DOE-2 algorithm are higher than those calculated using the coupling method for a large portion of the

time steps. Additionally, these differences increase with increasing wind speed. In practice, these findings impact architectural and engineering design by informing façade optimization against wind conditions, improving comfort, and reducing energy needs, particularly in high-wind regions. Further, these insights can be used for more accurate energy predictions and HVAC recommendations, which are critical in windy urban settings to avoid underestimating or overestimating heating and cooling requirements.

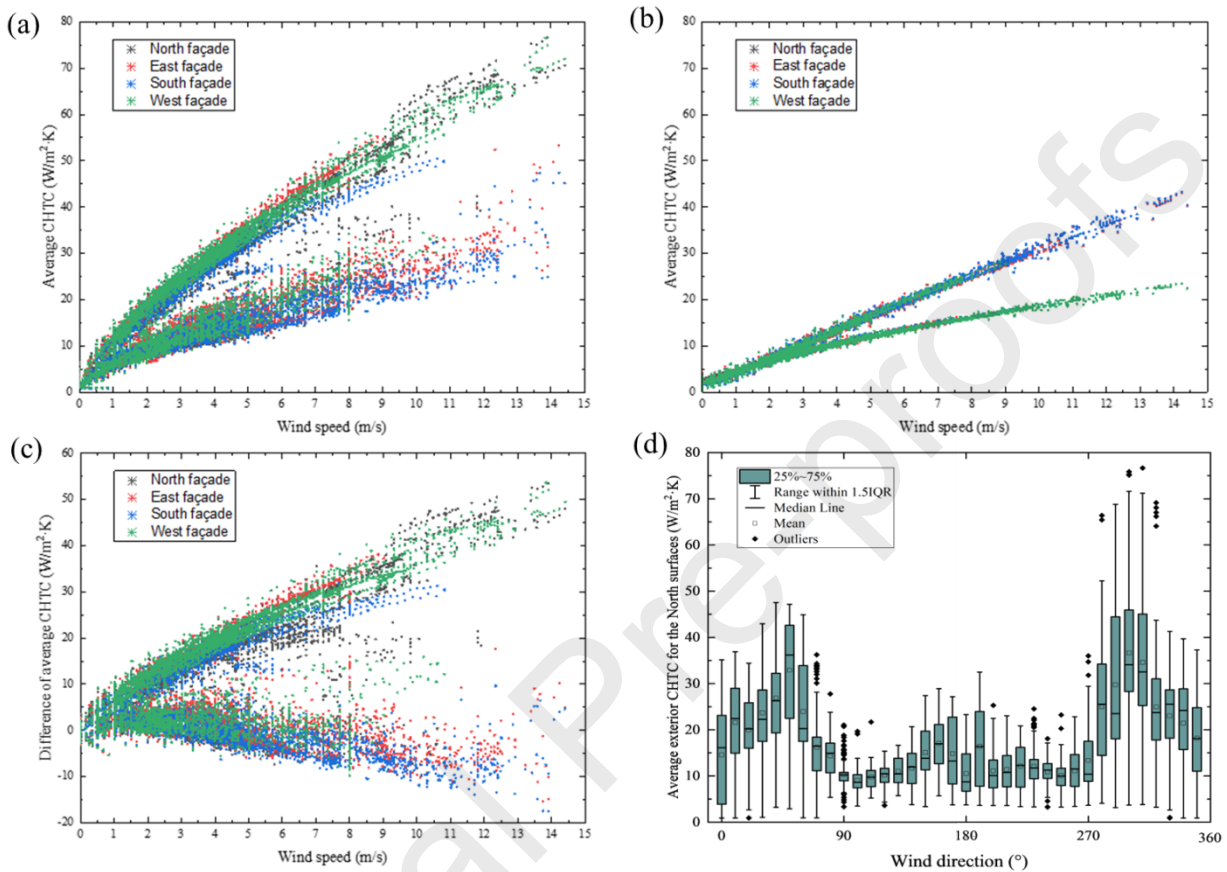


Figure 8 Average exterior CHTC of each oriented surface of (a) the coupling method and (b) the DOE-2 algorithm, (c) the difference between the two methods, and (d) average exterior CHTC for the north surface under different wind directions predicted by the coupling method.

Figure 8(d) **Error! Reference source not found.** shows a box plot of the average CHTC for the north façades against wind direction for each time step. The plot indicates a significant variability in CHTC values with wind direction. This aligns with the study's emphasis on the impact of diverse wind environments on high-rise buildings, which are often not adequately represented in standard BES tools. The range of CHTC values is visually depicted within the interquartile range (IQR) for each wind direction, highlighting the necessity of incorporating dynamic CHTC values in BES for accuracy. The presence of outliers and their distribution across different wind directions point to irregular conditions where the CHTC deviates substantially from the norm. These outliers, along with the mean values, suggest that certain wind directions may induce unique microclimates around the building, thus affecting its energy performance. This highlights the importance of considering these variations during the design phase to optimize energy performance, particularly in the heating season where higher CHTC values are consistent.

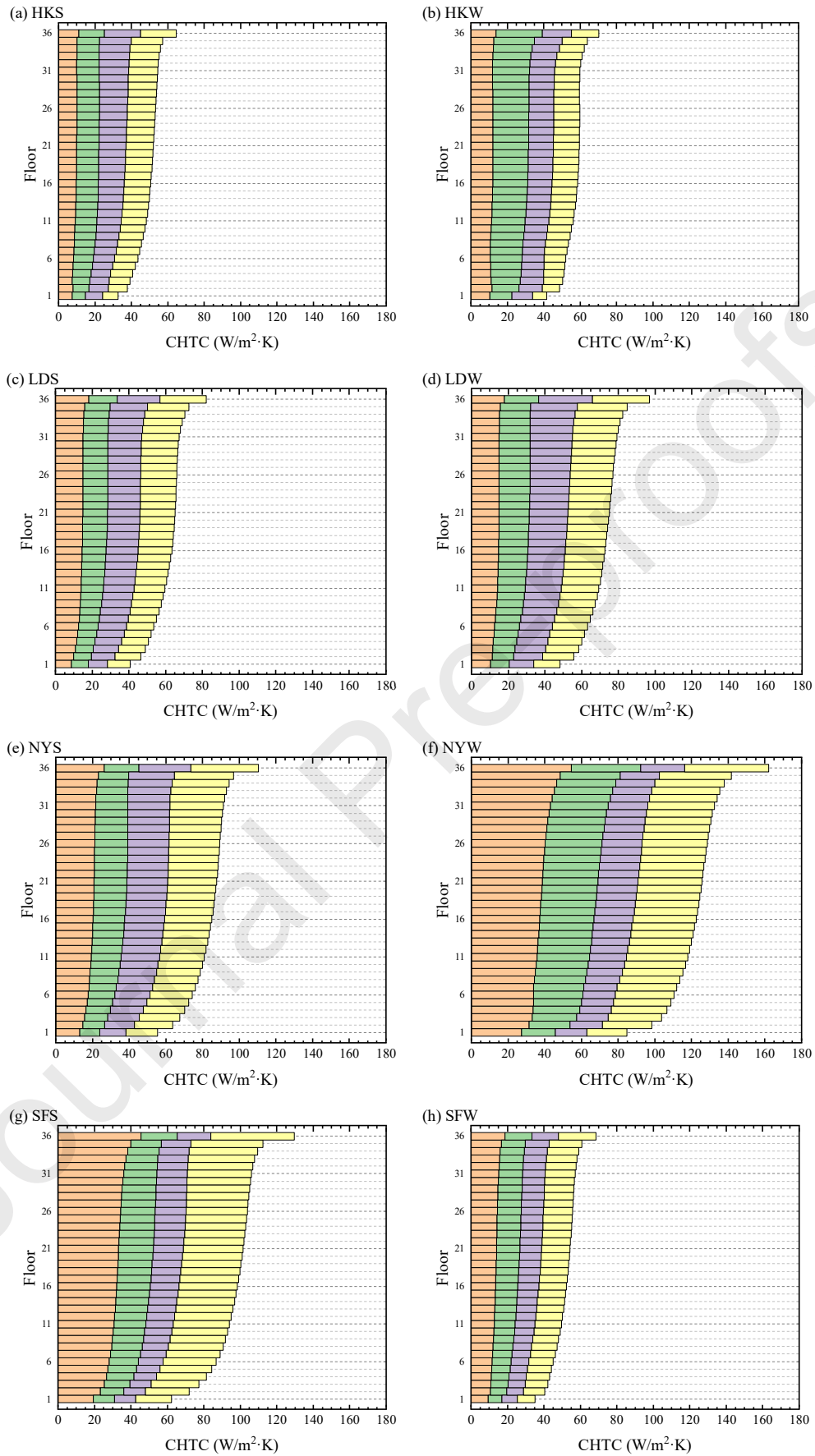
4.2 Exterior CHTC on high-rise buildings

Figure 9 shows the average CHTC values of the high-rise building located in five locations during the simulation periods for each floor, with the CHTC values split into different orientations. Due to differences in weather conditions, the CHTC values vary significantly between summer and winter periods and among different locations. Buildings located in Hong Kong (HK), London (LD), and New York (NY) have larger CHTC values in winter. In addition, the building in San Francisco (SF) generally has higher CHTC values during the summer, while the building in New York has higher CHTC values during the winter compared to other cities. The CHTC values also vary depending on the wall's orientation (North, East, South, or West).

The average CHTC values of all vertical surfaces in the high-rise building, calculated using the coupling method, are higher than those calculated using the DOE-2 algorithm in EnergyPlus (refer to Figure 10). This indicates an underestimation of overall convective heat transfer on the building façades by the DOE-2 algorithm. Additionally, the variations in CHTC between the coupling method and the DOE-2 algorithm differ across façade orientations due to varying wind speeds and directions among the cases. The underestimation of CHTC by the DOE-2 algorithm during the winter periods in London, New York, and Shanghai indicates that more heat is being lost from the buildings than the models predict, suggesting a potential need for improved insulation to reduce this heat loss during the colder months.

Figure 11 compares the average CHTC of all vertical exterior building surfaces during the simulation periods using both the coupling method and DOE-2 algorithms. Generally, as wind speed increases with building height, it is observed that CHTC also increases with the height for calculations made using both the coupling method and the DOE-2 algorithm. The total average CHTC calculated with the DOE-2 algorithm exhibits a consistent trend across all cases; however, there is a notable variation at the bottom of the building, and the rate of increase in CHTC diminishes as the floor height increases. Conversely, for the total average CHTC calculated using the coupling method, the increases at the base of the building are more pronounced, and the total average CHTC significantly rises towards the top of the building. According to the results, the value of CHTC on the leeward side façades does not increase uniformly with building height. Consequently, the total average CHTC calculated using the coupling method shows a more gradual increase on the upper middle floors.

Noteworthy are the significant disparities between the coupling method and the DOE-2 algorithm across seasons and locations. Particularly during summer periods, compared with the DOE-2 algorithm, the coupling method consistently records higher CHTC values, with differences ranging from 65.68% in London to 99.67% in Hong Kong. This trend is similar during winter periods, where the coupling method calculates greater CHTC values than the DOE-2 algorithm by percentages ranging from 69.11% in Hong Kong to 102.26% in Shanghai.



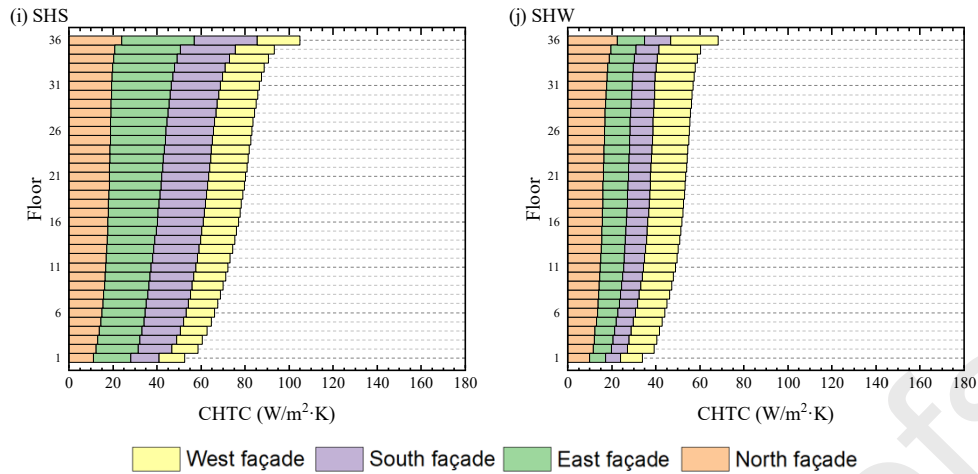


Figure 9 Average CHTC for Hong Kong, London, New York, San Francisco, and Shanghai summer (a, c, e, g, i) and winter (b, d, f, h, j).

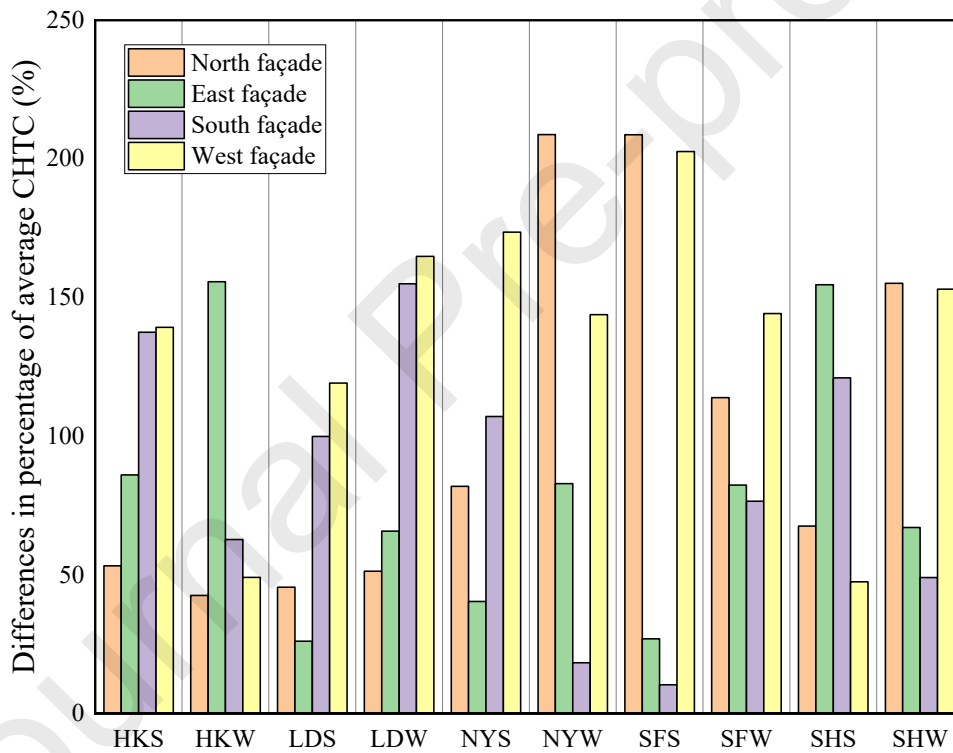


Figure 10 Comparison of average CHTC differences in percentage on different oriented façades between the coupling method and DOE-2 algorithm.

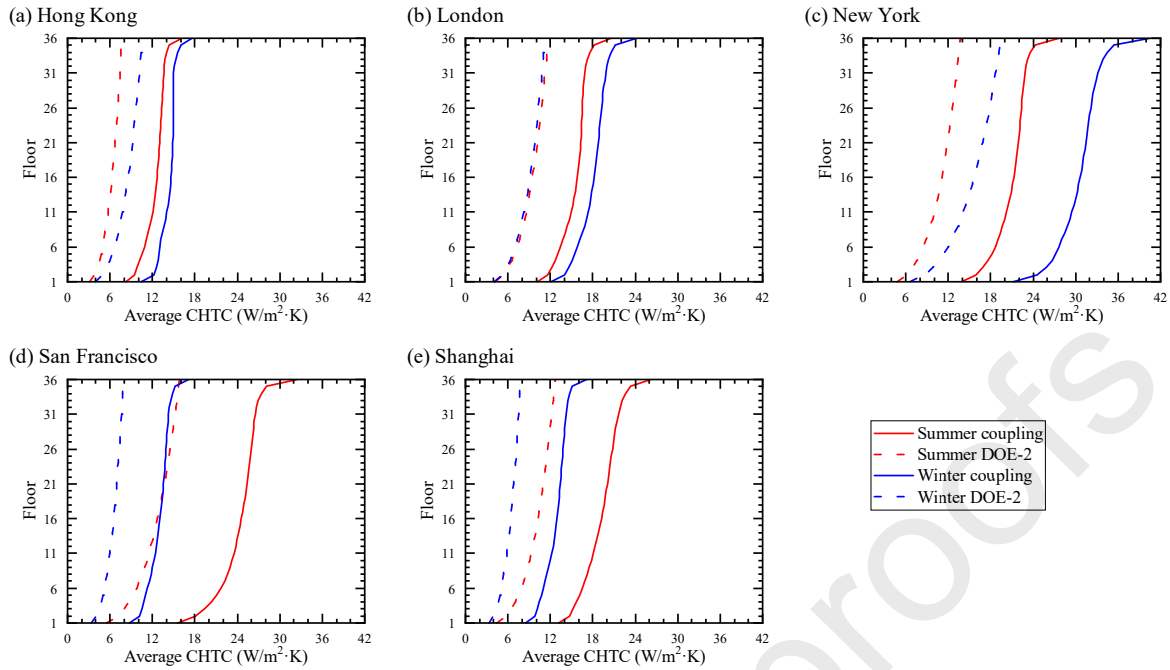


Figure 11 Comparison of average CHTC values of all vertical surfaces of the high-rise buildings along the building height located in (a) Hong Kong, (b) London, (c) New York, (d) Shanghai, (e) San Francisco between the coupling method and DOE-2 algorithm.

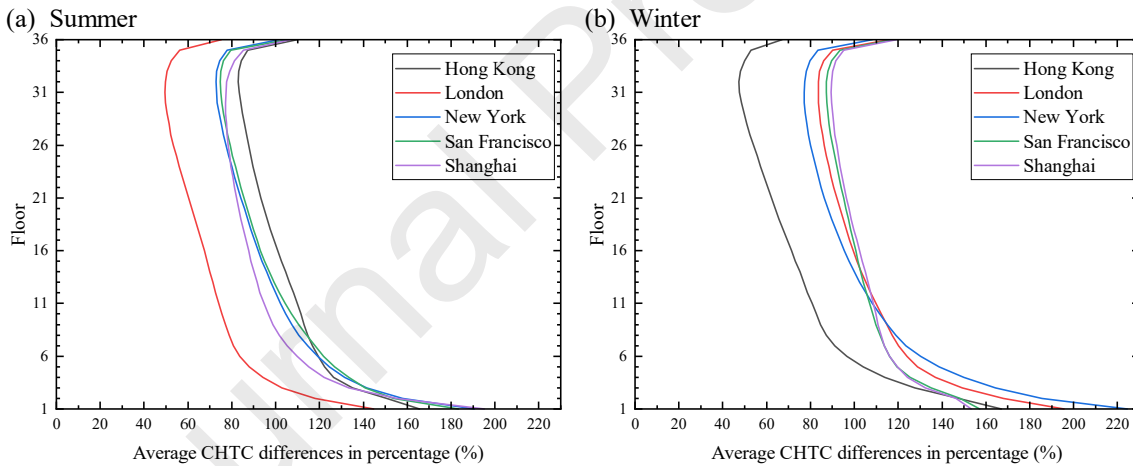


Figure 12 CHTC differences between coupling method and DOE-2 algorithm in percentage for (a) summer and (b) winter periods along the building height.

Figure 12 shows the differences in the percentage of average CHTC values of all the vertical façades using the coupling method and the DOE-2 algorithm along the building height for (a) summer and (b) winter periods. All cases show that the differences in average CHTC are greater near the lower and top floors of the building. For the middle floors, the differences in the average CHTCs decrease along the building height. Additionally, the differences in the winter periods are greater than those in the summer periods for all the locations, with the average differences being 92.57% in summer and 98.49% in winter.

The average CHTCs of all building surfaces using the coupling method and various algorithms in EnergyPlus during the Hong Kong summer with a low average local wind speed of 2.03 m/s and New York winter with a high average local wind speed of 6.60 m/s are illustrated in Figures 13(a) and (b), respectively. The average CHTC values calculated using different algorithms in EnergyPlus across

various cities and seasons show a consistent pattern. Most algorithms, including DOE-2, TARP, MoWiTT, and the Adaptive Convection Algorithm, underestimate the CHTC values compared to the coupling method. The Simple Combined algorithm, however, overestimates the values because it accounts for both convective and radiative heat transfer, resulting in higher CHTC outputs. Figure 13(c) presents the differences in the percentage of average CHTCs between the coupling method and various algorithms in EnergyPlus across different locations and seasons. This underestimation is uniform across various locations and seasons. The largest underestimations are observed with the Adaptive Convection Algorithm, with an average of 82.69% across all cases. This is followed by average underestimations of 71.76% for TARP, 58.55% for MoWiTT, and 47.47% for DOE-2. The Simple Combined algorithm has an average overestimation of 17.25%. Although the Simple Combined algorithm shows a consistent overestimation across most cases, in the New York winter period, it transitions to underestimation, whereas the underestimations by other algorithms are most significant. It should be noted that the heat transfer coefficient values for the Simple Combined algorithm include radiation.

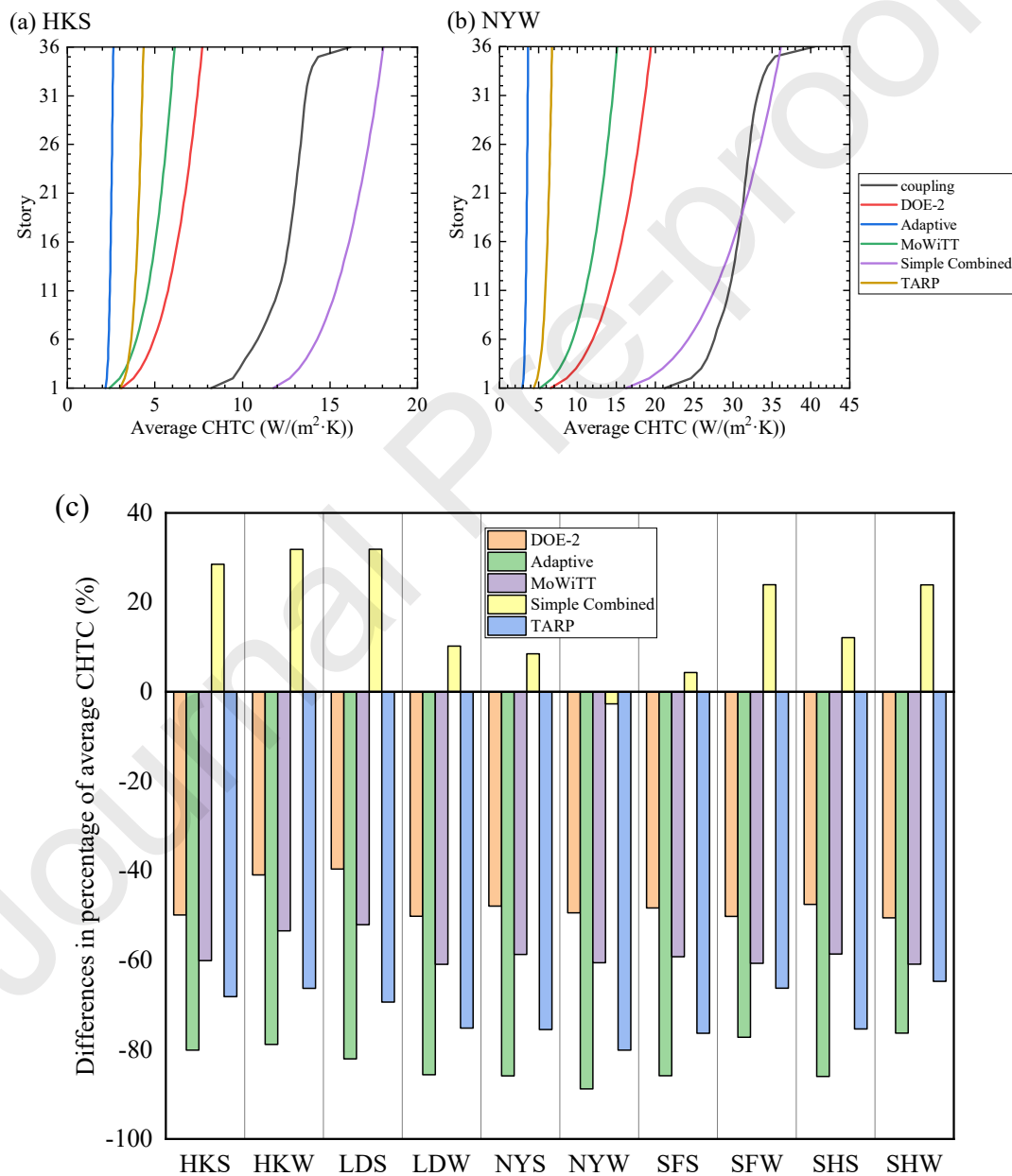
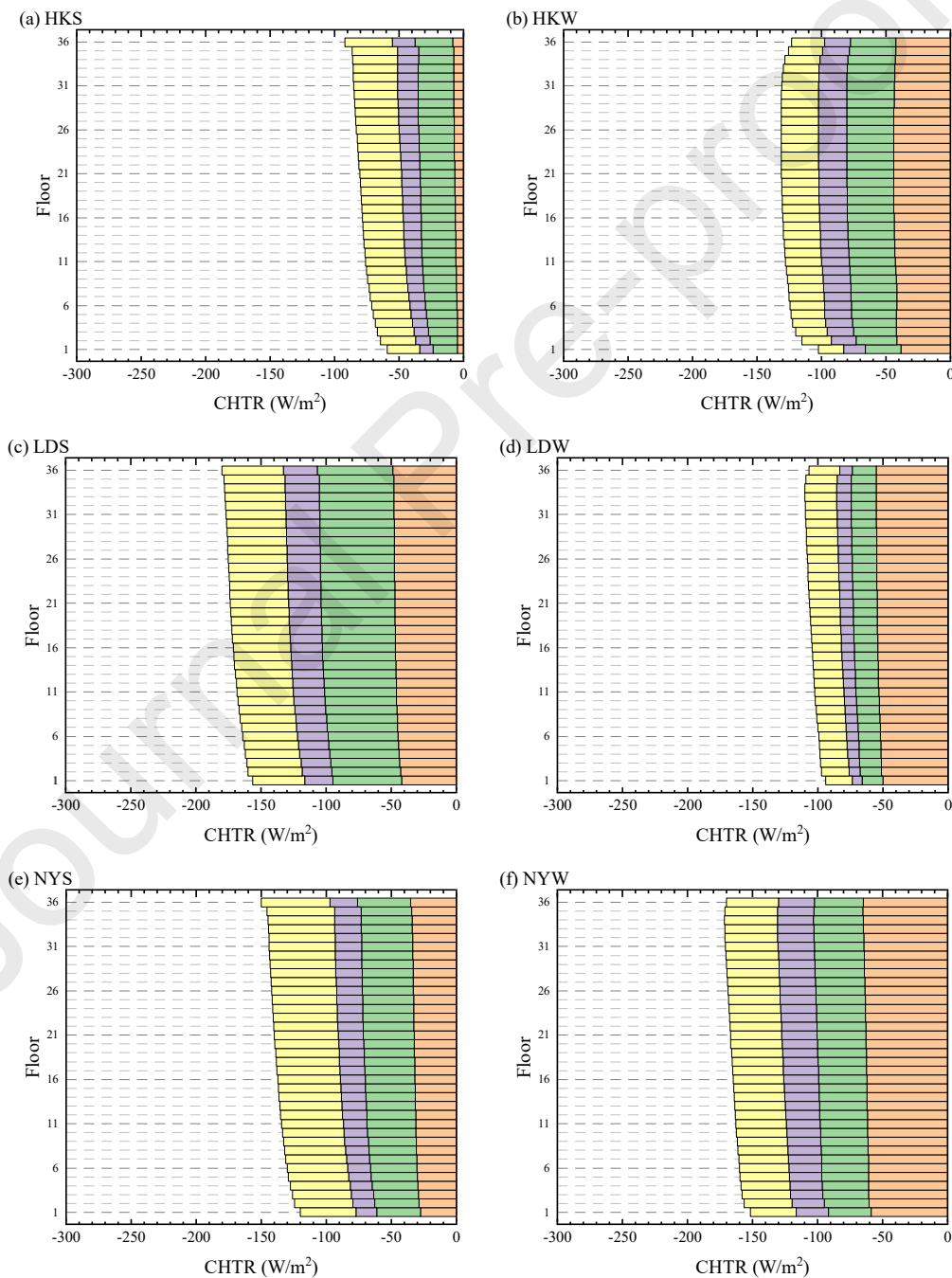


Figure 13 Average CHTCs for coupling method and algorithms in EnergyPlus during (a) Hong Kong summer and (b) New York winter, (c) Differences in percentage in average CHTCs between the coupling method and algorithms in EnergyPlus.

4.4 Comparison of CHTR using coupling method and DOE-2 algorithm

Figure 14 illustrates the exterior convective heat transfer rate (CHTR) for the high-rise building located in five different locations during the simulation periods for each floor. This figure provides a visual representation of how CHTR varies with height and seasonal conditions, offering insights into the thermal dynamics of high-rise buildings. Overall, the values of convective heat loss increase along with the building height, which aligns with the trends observed in CHTC calculations. However, in some cases, these values slightly decrease near the top of the building due to the wind direction during the simulation periods, as previously discussed in section 4.1. This phenomenon is observed in winter for locations such as Hong Kong, London, Shanghai, and San Francisco, as well as during the summer period in San Francisco.



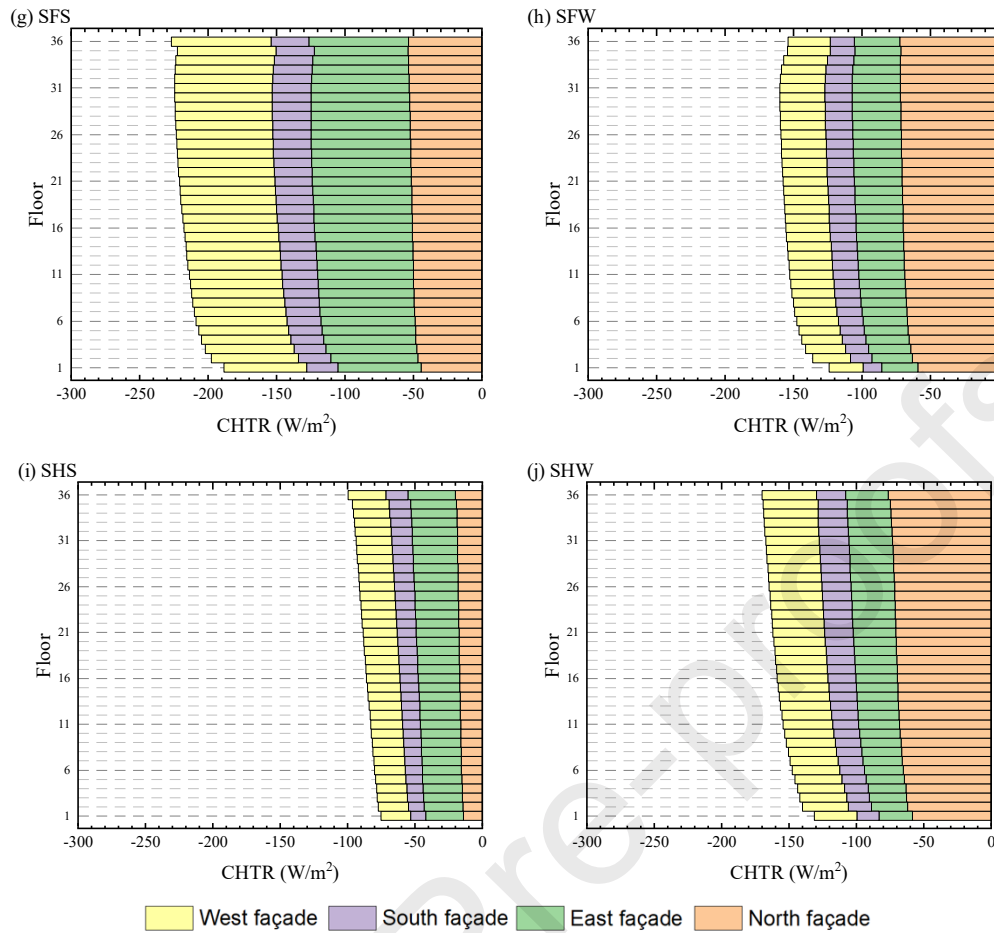


Figure 14 CHTR for Hong Kong, London, New York, San Francisco, and Shanghai summer (a, c, e, g, i) and winter (b, d, f, h, j).

As CHTR is calculated based on the CHTC and the temperature differences between the exterior building surface and the surrounding air, the variations in CHTR differ from those in CHTC, particularly in terms of directionality. For example, the east and west façades exhibit greater convective heat loss during the summer, while the north façade experiences greater convective heat loss during the winter across all locations. Additionally, as the exterior wall temperature is higher than the surrounding air, the building façades lose heat through convection.

These insights are crucial for informing building design and energy efficiency strategies across different locations and seasons. For example, enhancing the thermal performance of building façades at higher floors and optimizing certain orientations can lead to energy efficiencies. Such strategies could include tailored insulation materials, advanced façade technologies, or architectural features designed to mitigate unwanted heat loss or gain, thereby aligning more closely with the unique environmental conditions each building faces.

Figure 15(a) shows the differences in the percentage of average CHTRs of the different oriented façades using the coupling method and DOE-2 algorithm. On average, the utilization of the coupling method yields an average CHTR that is 18.64% higher compared to the results calculated using the DOE-2 algorithm. The differences in the percentage of average CHTRs vary across different seasons and locations. Shanghai's winter period had the greatest average CHTR difference percentage between the coupling method and the DOE-2 model. Hong Kong's summer and San Francisco's summer periods show uneven differences, with two oriented façades having greater differences compared to the other two oriented façades. Figure 15(b) shows the differences in the percentage of average CHTRs along the building height using the coupling method and DOE-2 algorithm. There are greater differences in the

percentage of average CHTR during the winter than during the summer. These differences tend to increase along with the building height, except on the top floor, and decrease more rapidly at the lower heights of the building.

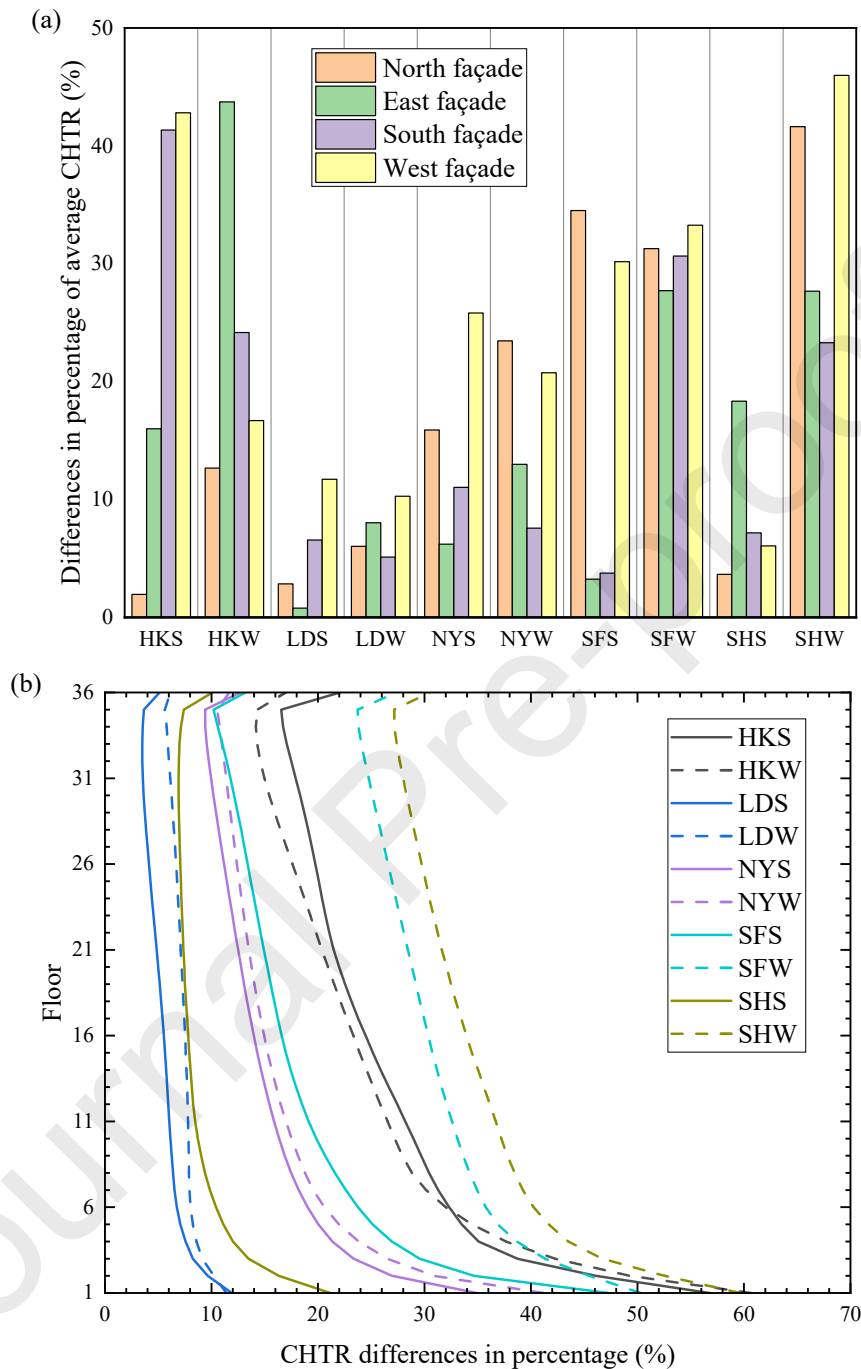


Figure 15 (a) Differences in percentage of average CHTRs of the different oriented façades using coupling method and DOE-2 algorithm and (b) Differences in percentage of average CHTRs along the building height between the coupling method and DOE-2 algorithm.

4.5 Comparison of outside surface heat balance using coupling method and DOE-2 algorithm

Figure 16(a) shows the difference in external wall heat gain rate per area for Hong Kong, London, New York, Shanghai, and San Francisco during the summer and winter periods between the coupling method and DOE-2 algorithm. The decreases in convection heat gain rate are due to the increase in CHTC values on the external surfaces directly for the coupling method. Although the coupling method only modified the CHTC values, it affected the whole external wall heat balance as the surface temperature of the external façades changed accordingly. The increase in convective heat loss led to less conduction heat loss as well as heat loss to the surroundings through the longwave radiation.

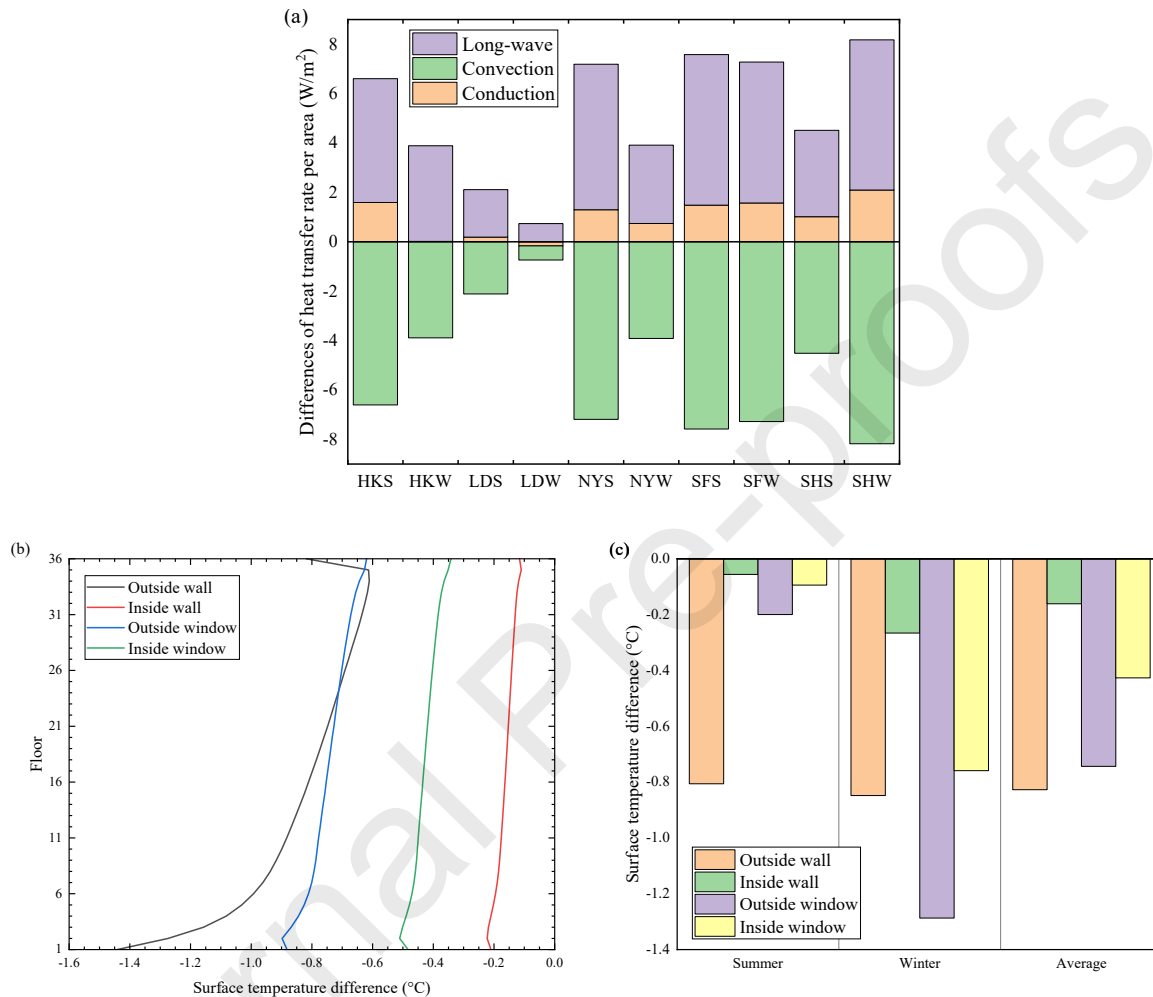


Figure 16 (a) Difference in external wall heat balance for five locations, (b) outside and inside surfaces temperature differences along with the building height, and (c) seasonal breakdown between the coupling method and DOE-2 algorithm.

Therefore, by changing the CHTC values using the coupling method, it is observed that the outside surface temperature as well as the inside surface temperature, were also affected, as shown in Figures 16(b) and (c). The temperature difference on the exterior wall surface shows a decreasing pattern with increasing height, except for the top floor. The temperature differences in the lower levels vary greatly, and they gradually diminish along with the building height. Meanwhile, the surface temperature of the wall inside steadily decreases from the first to the top floor. Both the window outside and inside surface temperatures show a similar decreasing trend. The coupling method consistently calculates lower temperatures compared to the DOE-2 algorithm across all floors, with the differences being more pronounced during winter conditions.

4.6 Comparison of heating/cooling energy using coupling method and algorithms

Figure 17 illustrates the differences in heating and cooling loads calculated using the coupling method compared to algorithms used in EnergyPlus, including DOE-2, the Adaptive Convection Algorithm, MoWiTT, Simple Combined, and TARP, across five locations with varied climate and wind conditions. The high-rise building analyzed in this study is designed with high-standard thermal performance for its building fabric, leading to higher cooling demands during the summer period and lower heating demands during the winter period. Greater percentage differences in winter heating loads are observed compared to summer cooling loads, indicating a higher variance in the performance of different algorithms during colder months.

Among the five algorithms used in EnergyPlus, the Simple Combined algorithm generally predicts lower heating and cooling loads than the coupling method due to its calculation of higher CHTC values. It shows the least differences in the prediction of heating and cooling loads, with an average of 4.30% lower energy demand compared to the coupling method. However, it predicts 35.69% more cooling loads in San Francisco during the summer because San Francisco has the highest average wind speed, causing the CHTC values calculated by the coupling method to be larger than those calculated by the Simple Combined algorithm. Despite this, other algorithms show a consistent trend in terms of differences in percentage for both heating and cooling loads. DOE-2 exhibits fewer differences in the prediction of heating/cooling load compared to the coupling method, ranging from 0.30% to 29.08%, followed by MoWiTT, TARP, and the Adaptive Convection Algorithm.

These findings reveal the varied effectiveness of the coupling method in buildings located in different cities with diverse climate conditions, particularly during the winter heating period. The discrepancies between the coupling method and other algorithms can vary significantly depending on the location and season. This variation highlights the importance of considering local climate conditions and seasonal variations when evaluating and selecting energy calculation methods for high-rise buildings.

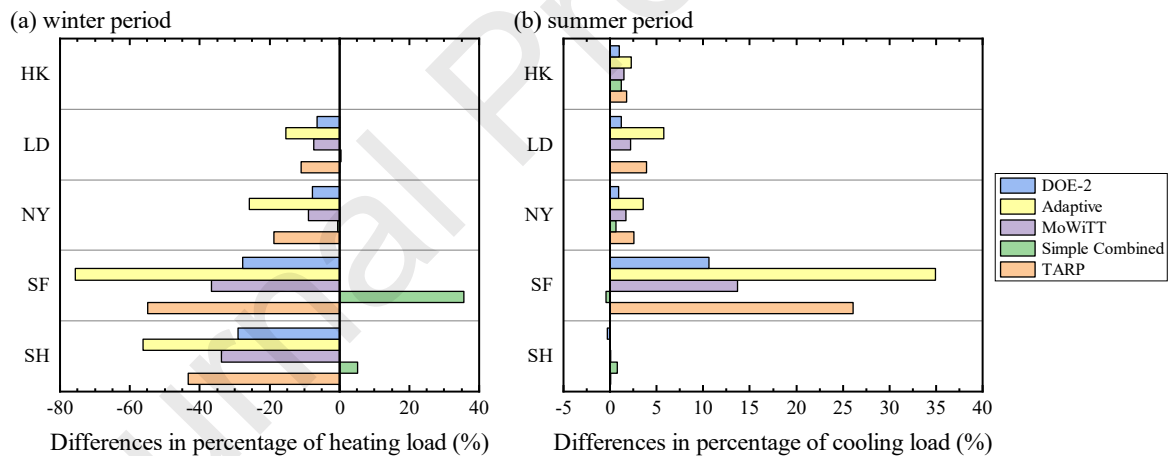


Figure 17 Difference in percentage of (a) heating and (b) cooling loads between EnergyPlus algorithms and coupling method.

5. Discussion and further considerations

5.1 Comparison with previous CFD studies

The exterior CHTC distribution across the windward façade of high-rise buildings using CFD was simulated during the co-simulation in the present study. The CFD results for a wind direction of 0° align with those from previous studies [16-18]. Overall, the CHTC increases from bottom to top and from the middle of the façade to the sides [18]. The highest CHTC values can be found at the top edge. A relatively uniform CHTC distribution was observed over the central part of the windward façade, corresponding to the uniform high-pressure and low-velocity zones in this part of the façade. The CHTC is relatively low in the lower part of the façade due to the horseshoe vortex [16].

Based on Kahsay et al. [17], for wind directions ranging from 0° to 45° towards the windward façade of a high-rise building, lower CHTCs are distributed at the bottom of the building. As the wind direction increases from 45° to 90° , the lower CHTCs at the bottom shift slightly upwards, forming a lower CHTC region on the 2nd floor, while a higher CHTC region forms in the middle of the building. The CHTC distribution on the windward façade is relatively insensitive to changes in wind direction. This can also be seen in Figure 7, where the CHTC distribution on the windward façade is similar to that when the wind direction is 0° . However, on the other façades, the effect of wind direction is more pronounced [18].

5.2 Reliability of the coupling method

Validated CFD models have been used to develop predictions for exterior CHTC, with accuracy steadily improving in recent years [9]. However, these models are generally more accurate for windward façades and less so for leeward façades. This discrepancy arises because steady RANS modeling cannot fully capture the inherently transient behavior of flow separation, recirculation, and von Karman vortex shedding occurring downstream of the windward façade [18]. In this study, CFD was used to obtain exterior CHTC values for all façades with different orientations, including windward, leeward, and the roof. This indicates that exterior CHTC values calculated using CFD for the leeward façades and roofs may still be inaccurate.

High-quality data for validating models that calculate exterior CHTC is essential [9]. Tian et al. [11] also emphasized the importance of validating the coupling model. The current general practice assumes the correctness and capability of the BES and CFD programs, validating them separately without providing a dedicated validation for the coupling model [6, 11]. Therefore, implementing more rigorous validation in future research can help evaluate the performance of co-simulation models. However, the current methodology for the coupling method is flexible; a developed CFD model in the future for better prediction of exterior CHTC can still be applied within this framework, increasing the accuracy of the co-simulation model.

5.3 Significance of buoyancy effect

The CHTCs in this study are calculated in Fluent without considering the buoyancy effect. However, in urban environments, the façades of high-rise buildings often experience significant thermal plumes, particularly during periods with little to no wind. These thermal plumes result from natural convection as warmer air rises along the building surfaces, influenced by vertical temperature gradients. This effect is critical in determining the overall heat transfer from the building's surfaces, impacting both energy consumption and thermal comfort.

To address this, initial simulations were conducted to test the influence of the buoyancy effect. Based on weather data, Hong Kong summer and San Francisco winter exhibit lower average wind speeds during simulation periods, while London winter represents average wind speeds among the locations, making these three scenarios suitable for studying the buoyancy effect. Figures 18 (a), (b), and (c) show the differences in average CHTC of all the building surfaces against wind speed during the simulation periods, representing the difference in CHTC when considering the buoyancy effect compared to when it is neglected.

Under low wind speed conditions (0 to 3 m/s), the buoyancy effect significantly increases CHTC values, especially during winter conditions. As wind speed increases beyond 3 m/s, the difference in average CHTCs gradually diminishes. Despite differences in cities and seasons, the impact of the buoyancy effect on the heat transfer coefficient under low wind speeds follows a similar pattern.

Although overlooking the effects of natural convection under calm wind conditions may limit the applicability of the findings in this study, in cases with higher average wind speeds, the proportion of low wind speed periods decreases, reducing the overall underestimation of CHTC. This approach will be applied to other cases in the present study. The average CHTC, CHTR, and heating or cooling loads

were compared while considering the buoyancy effect, as shown in Figures 18 (d), (e), and (f), respectively. Including the buoyancy effect results in fewer differences between the Simple Combined algorithm.

The results highlight the necessity of incorporating natural convection effects in thermal performance simulations to obtain more accurate predictions, especially in low wind speed environments. Future research should explore the influence of different building forms on the buoyancy effect and its impact on CHTC under varying climatic conditions.

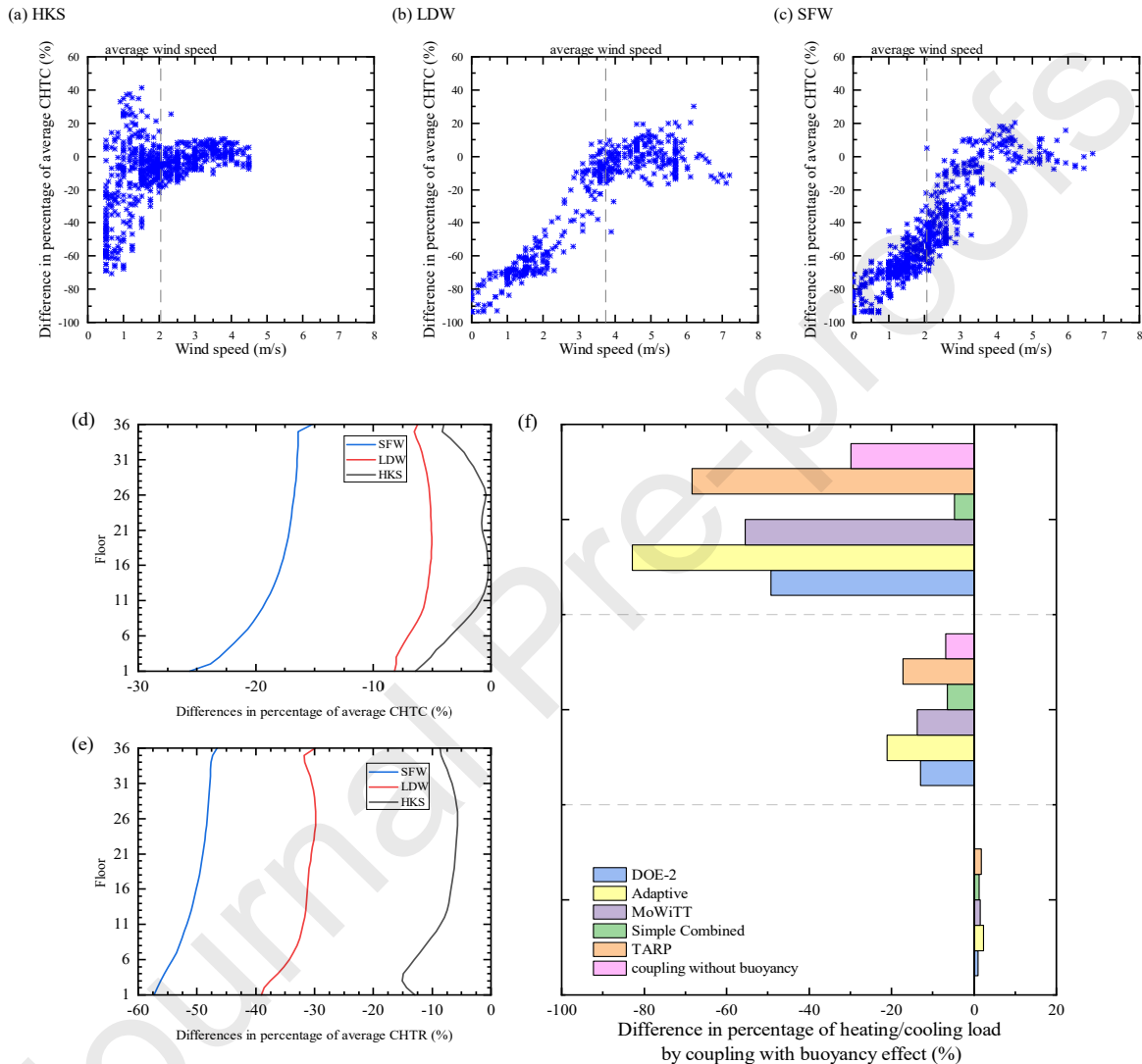


Figure 18 Average CHTC differences against wind speed for (a) Hong Kong summer, (b) London winter, and (c) San Francisco winter between coupling with and without buoyancy effect, differences in percentage of (d) average CHTC and (e) average CHTR, and (f) difference in percentage of heating/cooling load by coupling with buoyancy effect.

6. Conclusion and future works

In conclusion, this study reveals the complex relationship between wind patterns and convective heat transfer coefficients (CHTC) in high-rise building façades. Based on CFD simulation, CHTC increases significantly with building height. The variations are more significant at higher wind speeds. It is also

influenced by wind direction, with windward, leeward and backward façades responding differently to various wind conditions. The coupling method, integrating building energy simulation with computational fluid dynamics, proves effective in understanding CHTC variations under different wind conditions.

The study compares CHTC values calculated using the coupling method and the algorithm used in EnergyPlus across different seasons and locations. This discrepancy in CHTC between the coupling method and algorithms used in EnergyPlus varies across different orientations and seasons. For instance, the coupling method records higher CHTC values by 65.68% to 99.67% in summer and 69.11% to 102.26% in winter compared to the DOE-2 algorithm. Buildings in Hong Kong, London, and New York exhibit larger differences in the prediction of CHTC values in winter, while for San Francisco, higher differences occur in summer. The coupling method reveals substantial underestimations in the calculation of CHTC by traditional algorithms, particularly in winter.

The average CHTC values calculated using different algorithms in EnergyPlus across various cities and seasons show a consistent pattern. Most algorithms, including DOE-2, TARP, MoWiTT, and the Adaptive Convection Algorithm, underestimate CHTC values compared to the coupling method, except for the Simple Combined algorithm, which overestimates the values. The largest underestimations are observed with the Adaptive Convection Algorithm, averaging 82.69% across all cases, followed by average underestimations of 71.76% for TARP, 58.55% for MoWiTT, and 47.47% for DOE-2. The Simple Combined algorithm has an average overestimation of 17.25%.

The study also compares the exterior convective heat transfer rate (CHTR) and heating/cooling loads, which were calculated using different algorithms. The coupling method shows an 18.64% higher average CHTR compared to the DOE-2 algorithm, with significant seasonal and locational variations.

Among the various algorithms used in EnergyPlus for five locations during the summer and winter periods, the Simple Combined algorithm calculates 4.30% lower energy demand. In contrast, other algorithms calculate higher energy demand, with DOE-2 being the closest to the coupling method, showing a 5.76% overestimation. This is followed by MoWiTT with a 6.77% overestimation, TARP with 9.37%, and the Adaptive Convection Algorithm with 12.63%. The discrepancies between the coupling method and other algorithms can vary significantly depending on the location and season. This variation highlights the importance of considering local climate conditions and seasonal variations when evaluating and selecting energy calculation methods for high-performance high-rise buildings.

Overall, this research emphasizes the necessity of integrating detailed wind modeling into BES tools for more accurate predictions of thermal loads and energy performance in high-rise buildings. The findings inform architectural and engineering design, particularly in optimizing façades against wind conditions to enhance comfort and reduce energy needs in urban environments.

Despite the significant computational time and power required, the depth and accuracy of the data generated justify the investment, particularly for detailed studies focused on enhancing building design and energy efficiency. Given the computational intensity of the CFD simulations, direct application in standard practice might be impractical for all but the most critical projects. However, the method's value in a research context is substantial, providing detailed insights that can improve predictive accuracy for building energy simulations.

Building on the findings of this study, future research should explore several key areas to further enhance the accuracy and applicability of CFD-BES coupling methods in high-rise buildings. One promising direction is the integration of machine learning algorithms to predict CHTC values based on a combination of CFD simulation results and real-world data. Once such datasets reach a critical mass, machine learning could play a significant role in predicting CHTC based on shorter-term or less computationally demanding simulations, offering a promising compromise between computational load and simulation accuracy. Additionally, future studies should investigate the impact of varying building geometries and façade designs on convective heat transfer under different climatic conditions, including

the effects of natural ventilation and dynamic shading devices. The inclusion of buoyancy effects and detailed microclimate interactions, especially in urban canyon environments, will also be crucial in refining the models. Finally, extensive experimental validation using data from instrumented high-rise buildings in diverse climates will be essential to verify and calibrate the simulation models.

CRedit authorship contribution statement

Kemin Ding: Conceptualization, Methodology, Software, Validation, Formal analysis, Investigation, Data Curation, Visualization, Writing - original draft, Writing - review & editing. **John Kaiser Calautit:** Conceptualization, Methodology, Investigation, Supervision, Resources, Writing - review & editing. **Carlos Jimenez-Bescos:** Writing - review & editing, Investigation.

Declaration of competing interest

The authors declare that they have no known competing financial interests or personal relationships that could have appeared to influence the work reported in this paper.

Acknowledgement

The authors would like to thank the support of the Department of Architecture and Built Environment of the University of Nottingham for providing the facility for carrying out the modelling and simulations.

References

- [1] J.K. Calautit, L. X. Yong, Fad or future? Navigating challenges and proposing holistic solutions in sustainable building design, *One Earth*, 6 (2023) 1430-1434, <https://doi.org/10.1016/j.oneear.2023.10.020>.
- [2] M. Singh, R. Sharston, A literature review of building energy simulation and computational fluid dynamics co-simulation strategies and its implications on the accuracy of energy predictions, *Building Services Engineering Research and Technology*, 43 (1) (2022) 113-138, [10.1177/01436244211020465](https://doi.org/10.1177/01436244211020465).
- [3] J.A. Palyvos, A survey of wind convection coefficient correlations for building envelope energy systems' modeling, *Applied Thermal Engineering*, 28 (8) (2008) 801-808, <https://doi.org/10.1016/j.applthermaleng.2007.12.005>.
- [4] R. Zhang, K.P. Lam, S.-c. Yao, Y. Zhang, Coupled EnergyPlus and computational fluid dynamics simulation for natural ventilation, *Building and Environment*, 68 (2013) 100-113, <https://doi.org/10.1016/j.buildenv.2013.04.002>.
- [5] P. Shen, M. Dai, P. Xu, W. Dong, Building heating and cooling load under different neighbourhood forms: Assessing the effect of external convective heat transfer, *Energy*, 173 (2019) 75-91, <https://doi.org/10.1016/j.energy.2019.02.062>.
- [6] Z. Zhai, Q. Chen, P. Haves, J.H. Klems, On approaches to couple energy simulation and computational fluid dynamics programs, *Building and Environment*, 37 (8) (2002) 857-864, [https://doi.org/10.1016/S0360-1323\(02\)00054-9](https://doi.org/10.1016/S0360-1323(02)00054-9).

- [7] M. Zhang, Z. Gao, Effect of urban form on microclimate and energy loads: Case study of generic residential district prototypes in Nanjing, China, *Sustainable Cities and Society*, 70 (2021) 102930, <https://doi.org/10.1016/j.scs.2021.102930>.
- [8] M.S. Fernandes, E. Rodrigues, J.J. Costa, A new wind direction-driven heat convection model is needed in dynamic simulation: What, why, and how, *Energy and Buildings*, 256 (2022) 111716, <https://doi.org/10.1016/j.enbuild.2021.111716>.
- [9] M. Mirsadeghi, D. Cóstola, B. Blocken, J.L.M. Hensen, Review of external convective heat transfer coefficient models in building energy simulation programs: Implementation and uncertainty, *Applied Thermal Engineering*, 56 (1-2) (2013) 134-151, [10.1016/j.applthermaleng.2013.03.003](https://doi.org/10.1016/j.applthermaleng.2013.03.003).
- [10] M.G. Emmel, M.O. Abadie, N. Mendes, New external convective heat transfer coefficient correlations for isolated low-rise buildings, *Energy and Buildings*, 39 (3) (2007) 335-342, <https://doi.org/10.1016/j.enbuild.2006.08.001>.
- [11] W. Tian, X. Han, W. Zuo, M.D. Sohn, Building energy simulation coupled with CFD for indoor environment: A critical review and recent applications, *Energy and Buildings*, 165 (2018) 184-199, [10.1016/j.enbuild.2018.01.046](https://doi.org/10.1016/j.enbuild.2018.01.046).
- [12] X. Yang, L. Zhao, M. Bruse, Q. Meng, An integrated simulation method for building energy performance assessment in urban environments, *Energy and Buildings*, 54 (2012) 243-251, <https://doi.org/10.1016/j.enbuild.2012.07.042>.
- [13] A.U. Weerasuriya, X. Zhang, V.J.L. Gan, Y. Tan, A holistic framework to utilize natural ventilation to optimize energy performance of residential high-rise buildings, *Building and Environment*, 153 (2019) 218-232, <https://doi.org/10.1016/j.buildenv.2019.02.027>.
- [14] Y. Pan, Y. Li, Z. Huang, G. Wu, Study on simulation methods of atrium building cooling load in hot and humid regions, *Energy and Buildings*, 42 (10) (2010) 1654-1660, <https://doi.org/10.1016/j.enbuild.2010.04.008>.
- [15] T. Defraeye, B. Blocken, J. Carmeliet, Convective heat transfer coefficients for exterior building surfaces: Existing correlations and CFD modelling, *Energy Conversion and Management*, 52 (1) (2011) 512-522, [10.1016/j.enconman.2010.07.026](https://doi.org/10.1016/j.enconman.2010.07.026).
- [16] H. Montazeri, B. Blocken, D. Derome, J. Carmeliet, J.L.M. Hensen, CFD analysis of forced convective heat transfer coefficients at windward building facades: Influence of building geometry, *Journal of Wind Engineering and Industrial Aerodynamics*, 146 (2015) 102-116, [10.1016/j.jweia.2015.07.007](https://doi.org/10.1016/j.jweia.2015.07.007).
- [17] M.T. Khasay, G.T. Bitsuamlak, F. Tariku, CFD simulation of external CHTC on a high-rise building with and without façade appurtenances, *Building and Environment*, 165 (2019) 106350, <https://doi.org/10.1016/j.buildenv.2019.106350>.
- [18] B. Blocken, T. Defraeye, D. Derome, J. Carmeliet, High-resolution CFD simulations for forced convective heat transfer coefficients at the facade of a low-rise building, *Building and Environment*, 44 (12) (2009) 2396-2412, <https://doi.org/10.1016/j.buildenv.2009.04.004>.
- [19] Y.K. Yi, N. Feng, Dynamic integration between building energy simulation (BES) and computational fluid dynamics (CFD) simulation for building exterior surface, *Building Simulation*, 6 (3) (2013) 297-308, [10.1007/s12273-013-0116-9](https://doi.org/10.1007/s12273-013-0116-9).
- [20] M. Miguel, W.N. Hien, I. Marcel, H.D. Jun Chung, H. Yueer, Y. Zhonqi, D. Ji-Yu, S.V. Raghavan, N.N. Son, A physically-based model of interactions between a building and its outdoor

conditions at the urban microscale, *Energy and Buildings*, 237 (2021) 110788,<https://doi.org/10.1016/j.enbuild.2021.110788>.

[21] R. Zhang, P.A. Mirzaei, B. Jones, Development of a dynamic external CFD and BES coupling framework for application of urban neighbourhoods energy modelling, *Building and Environment*, 146 (2018) 37-49,<https://doi.org/10.1016/j.buildenv.2018.09.006>.

[22] M. Gijón-Rivera, J. Xamán, G. Álvarez, J. Serrano-Arellano, Coupling CFD-BES Simulation of a glazed office with different types of windows in Mexico City, *Building and Environment*, 68 (2013) 22-34,<https://doi.org/10.1016/j.buildenv.2013.06.005>.

[23] T. Yamamoto, A. Ozaki, S. Kaoru, K. Taniguchi, Analysis method based on coupled heat transfer and CFD simulations for buildings with thermally complex building envelopes, *Building and Environment*, 191 (2021) 107521,<https://doi.org/10.1016/j.buildenv.2020.107521>.

[24] C.O.R. Negrão, Integration of computational fluid dynamics with building thermal and mass flow simulation, *Energy and Buildings*, 27 (2) (1998) 155-165,[https://doi.org/10.1016/S0378-7788\(97\)00036-4](https://doi.org/10.1016/S0378-7788(97)00036-4).

[25] I. Beausoleil-Morrison, The adaptive coupling of heat and air flow modelling within dynamic whole-building simulation, Department of Mechanical Engineering, University of Strathclyde, 2000.

[26] M. Bartak, I. Beausoleil-Morrison, J.A. Clarke, J. Denev, F. Drkal, M. Lain, I.A. Macdonald, A. Melikov, Z. Popiolek, P. Stankov, Integrating CFD and building simulation, *Building and Environment*, 37 (8) (2002) 865-871,[https://doi.org/10.1016/S0360-1323\(02\)00045-8](https://doi.org/10.1016/S0360-1323(02)00045-8).

[27] E. Djunaedy, J. Hensen, M. Loomans, Selecting an appropriate tool for airflow simulation in buildings, *Building Services Engineering Research and Technology*, 25 (3) (2004) 269-278,[10.1191/0143624404bt109oa](https://doi.org/10.1191/0143624404bt109oa).

[28] L. Wang, N.H. Wong, Coupled simulations for naturally ventilated residential buildings, *Automation in Construction*, 17 (4) (2008) 386-398,<https://doi.org/10.1016/j.autcon.2007.06.004>.

[29] S. Khoshdel Nikkho, M. Heidarinejad, J. Liu, J. Srebric, Quantifying the impact of urban wind sheltering on the building energy consumption, *Applied Thermal Engineering*, 116 (2017) 850-865,<https://doi.org/10.1016/j.applthermaleng.2017.01.044>.

[30] A. Mochida, H. Yoshino, S. Miyauchi, T. Mitamura, Total analysis of cooling effects of cross-ventilation affected by microclimate around a building, *Solar Energy*, 80 (4) (2006) 371-382,<https://doi.org/10.1016/j.solener.2005.08.014>.

[31] M.T. Khasay, G.T. Bitsuamlak, F. Tariku, Thermal zoning and window optimization framework for high-rise buildings, *Applied Energy*, 292 (2021) 116894,<https://doi.org/10.1016/j.apenergy.2021.116894>.

[32] M.T. Khasay, G. Bitsuamlak, F. Tariku, Effect of localized exterior convective heat transfer on high-rise building energy consumption, *Building Simulation*, 13 (1) (2020) 127-139,[10.1007/s12273-019-0568-7](https://doi.org/10.1007/s12273-019-0568-7).

[33] P. Shen, Z. Wang, How neighborhood form influences building energy use in winter design condition: Case study of Chicago using CFD coupled simulation, *Journal of Cleaner Production*, 261 (2020) 121094,<https://doi.org/10.1016/j.jclepro.2020.121094>.

- [34] E.R. Meinders, K. Hanjalic, R.J. Martinuzzi, Experimental Study of the Local Convection Heat Transfer From a Wall-Mounted Cube in Turbulent Channel Flow, *Journal of Heat Transfer*, 121 (3) (1999) 564-573, [10.1115/1.2826017](https://doi.org/10.1115/1.2826017).
- [35] M. Wetter, Co-simulation of building energy and control systems with the Building Controls Virtual Test Bed, *Journal of Building Performance Simulation*, 4 (3) (2011) 185-203, [10.1080/19401493.2010.518631](https://doi.org/10.1080/19401493.2010.518631).
- [36] I. Beausoleil-Morrison, The adaptive conflation of computational fluid dynamics with whole-building thermal simulation, *Energy and Buildings*, 34 (9) (2002) 857-871, [https://doi.org/10.1016/S0378-7788\(02\)00061-0](https://doi.org/10.1016/S0378-7788(02)00061-0).
- [37] CTBUH, *Cities Database*, in, 2024,
- [38] M. Deru, K. Field, D. Studer, K. Benne, B. Griffith, P. Torcellini, B. Liu, M. Halverson, D. Winiarski, M. Rosenberg, US Department of Energy commercial reference building models of the national building stock, (2011)
- [39] ASHRAE, *ASHRAE 90.1 2007 Energy Standard for Buildings Except Low-Rise Residential Buildings*, SI Edition, 2007.
- [40] ASHRAE, *ASHRAE 169-2020 Climatic Data for Building Design Standards*, 2010.
- [41] F. Zhong, J.K. Calautit, Y. Wu, Assessment of HVAC system operational fault impacts and multiple faults interactions under climate change, *Energy*, 258 (2022) 124762, <https://doi.org/10.1016/j.energy.2022.124762>.
- [42] EnergyPlus, *EnergyPlus Documentation Engineering Reference: the reference to EnergyPlus calculations*, US Department of Energy, 2020.
- [43] L.B. Laboratory, DOE2. 1E-053 source code, 1994.
- [44] ASHRAE, *ASHRAE Handbook: Fundamentals*, Atlanta: American Society of Heating, Refrigerating, and Air-Conditioning Engineers, Inc, 1989.
- [45] G.N. Walton, *Thermal analysis research program reference manual*, US Department of Commerce, National Bureau of Standards Washington, DC, USA, 1983.
- [46] E.M. Sparrow, J.W. Ramsey, E.A. Mass, Effect of Finite Width on Heat Transfer and Fluid Flow about an Inclined Rectangular Plate, *Journal of Heat Transfer*, 101 (2) (1979) 199-204, [10.1115/1.3450946](https://doi.org/10.1115/1.3450946).
- [47] M. Yazdanian, J.H. Klems, Measurement of the exterior convective film coefficient for windows in low-rise buildings, (1993)
- [48] A. Inc., *ANSYS Fluent User's Guide 2021 R1*, in, 2021,
- [49] S.M.A. Aftab, A.S. Mohd Rafie, N.A. Razak, K.A. Ahmad, Turbulence Model Selection for Low Reynolds Number Flows, *PLOS ONE*, 11 (4) (2016) e0153755, [10.1371/journal.pone.0153755](https://doi.org/10.1371/journal.pone.0153755).
- [50] Y. Tominaga, A. Mochida, R. Yoshie, H. Kataoka, T. Nozu, M. Yoshikawa, T. Shirasawa, AIJ guidelines for practical applications of CFD to pedestrian wind environment around buildings, *Journal of Wind Engineering and Industrial Aerodynamics*, 96 (10) (2008) 1749-1761, <https://doi.org/10.1016/j.jweia.2008.02.058>.

[51] P.J. Richards, S.E. Norris, Appropriate boundary conditions for computational wind engineering models revisited, *Journal of Wind Engineering and Industrial Aerodynamics*, 99 (4) (2011) 257-266, <https://doi.org/10.1016/j.jweia.2010.12.008>.

Declaration of interests

The authors declare that they have no known competing financial interests or personal relationships that could have appeared to influence the work reported in this paper.

The authors declare the following financial interests/personal relationships which may be considered as potential competing interests: